

We are IntechOpen, the world's leading publisher of Open Access books Built by scientists, for scientists

6,900

Open access books available

185,000

International authors and editors

200M

Downloads

Our authors are among the

154

Countries delivered to

TOP 1%

most cited scientists

12.2%

Contributors from top 500 universities



WEB OF SCIENCE™

Selection of our books indexed in the Book Citation Index
in Web of Science™ Core Collection (BKCI)

Interested in publishing with us?
Contact book.department@intechopen.com

Numbers displayed above are based on latest data collected.
For more information visit www.intechopen.com



Fractals in Antennas and Metamaterials Applications

Wojciech Jan Krzysztofik

Additional information is available at the end of the chapter

<http://dx.doi.org/10.5772/intechopen.68188>

Abstract

Recently, telecommunication systems have been requiring more advanced features in the design and operation. Among others a smaller size of devices, which can be integrated for multiple mobile communication systems, applied in one user's device board, such as PDA or smart phone. Moreover, the cost of mass production should be minimized as much as possible. To meet part of that request, the antennas of these devices should have small size, lower weight, operating in multiple frequency bands and/or be broadband. There are many research methods to achieve this goal, one of which is using the fractal geometries for the shape of antenna elements. In recent years, there are many fractal shapes that have been proposed for such applications, and the designed antennas have significantly improved antenna features such as smaller size, operating in multi-frequency bands, with improved power gain and efficiency. In recent years, the new approach for modern antenna the metamaterials, MTM, is adopted, and sometimes that based on the fractal geometry is adopted.

Keywords: fractal geometries, fractal dimension, IFS, fractal antenna, antenna elements, multiband, power gain, efficiency, compact size, antenna array, metamaterials, MTM

1. Introduction

Antenna structures are well known, it takes them a lot of research and development centres. Relatively rarely appearing solutions that represent a new approach in the view of the traditional methods of design are applied to modern radio communication systems [9]. So far, the antenna had simple shapes that are described in Euclidean geometry. In the past dozen years, many scientists around the world tried to make the structure of fractal geometry for applications in the field of electromagnetism, which led to the development of new innovative construction of antennas and artificial dielectric/magnetic materials, so-called metamaterials, MTM.

Structure based on fractal geometry cannot be described in the traditional Euclidean geometry. They are built with sequence of replicas based on the same shapes, which could be scaled, rotated and displaced in the space. In the research environment in the field of electromagnetism, intriguing was the answer to the question whether the properties of fractals can be useful in the design of elements of specific electromagnetic properties.

Fractals are abstract objects that, as satisfying in the strict sense of mathematical description, cannot be physically implemented, because these are infinite. However, you can make some assumptions in relation to the ideal fractal, which allow for constructing electromagnetic instruments, such as antennas, filters and microwave substrates having high surface impedance, circuit filters, electronic components of frequency-stop-band properties and others. Typically, these shapes are called pre-fractals or truncated fractals. You can apply different geometries, such as configurations of multiple triangles or other complicated constructions to build antennas that may be similar to fractal shapes and extract some of their advantages, which in theory can be obtained as a result of mathematical abstraction. Generally, the fractal antenna technology is a term used to describe these antenna engineering techniques, which are based on such mathematical concepts that provide generation of new antennas with some features that were not possible even in the mid-1980s.

To sum up the results of the work carried out so far, you can formulate the following benefits resulting from the application of the fractal technology:

1. Self-similarity is useful in the design of multi-frequency antenna, as, for example, the devices based on the Sierpinski fractal gasket or carpet, Minkowski fractal loop or patch that have been used in the design of multi-band antenna.
2. The self-filling property is useful for the design of electrically small antennas, such as Hilbert fractal, Peano fractal and Koch fractal monopoles or loops and the microstrip antennas.
3. The mass fractals and the boarder fractals are useful in obtaining high directivity and low sidelobes antenna elements and arrays.
4. Recently, the self-filling in space curves like Hilbert and Peano fractals were used to obtain high-impedance ground plane EBG, so-called metamaterials, used to design high performance, low profile, conformal antennas with enhanced radiation characteristics and improved power gain of various communication and radar applications.

Fractal geometry has many applications in life and open up new research directions in many fields such as biology and economics. In many EM devices, the self-similarity and plane-filling nature of fractal geometries are often qualitatively linked to its frequency characteristics, i.e. multi-frequency operation, or small size in low frequency bands. In addition, fractal geometries have been used in the electromagnetic radiation, and especially in the design of antennas with compact size and operating at multiband frequency. Some important characteristics of fractal geometries can be applied to design antenna. The self-similar design is used to operate the multi-band antenna. The self-space-filling structure of the fractal is used to design the small antennas. Mass fractals and boundary fractals are used to design array antennas.

1.1. Brief introduction to fractal geometry

The original inspiration for the development of fractal geometry came largely from an in-depth study of the patterns of nature (see **Figure 1**).

The fractals, for example, have been successfully applied to the modelling of complex objects found in nature, such as systems of galaxies and strokes of clouds, mountain ranges, coast-lines, snowflakes, trees, foliage plants and many others. By millions of years of evolution, nature optimizes architecture biological structures for effective distribution and use of energy, and, in principle, fractal shapes can be found in each of these structures.

Mandelbrot realized [10] that very often it is impossible to describe the objects that occur in nature using only Euclidean geometry, by means of straight lines, circles, cubes and the like. He proposed that fractals and fractal geometry can be used to describe real objects, such as trees, flashes of lightning, meandering rivers and coasts, to name just a few. Fractal dimensions need not be expressed using integers, so intuitively, we present them as a measure of how much space does the fractal occupies.

Fractals can be found in nature or could be generated using mathematical rules. Probably the easiest way to define a fractal is to describe it as an object, which is similar in varying degrees of zoom, and as a result, with the symmetry of the whole scale, with each a small part of the entire structure of the replacement object. Some examples of objects that have the characteristics of the self-similarity are shown in **Figure 2**.

Here are five properties, which most fractals have:

- They are made up of elements with any small scale,
- They are usually defined by a simple recursive processes,
- They are too irregular to be described using traditional Euclidian geometry,
- They have some type of self-similarity,
- They have fractal dimensions.

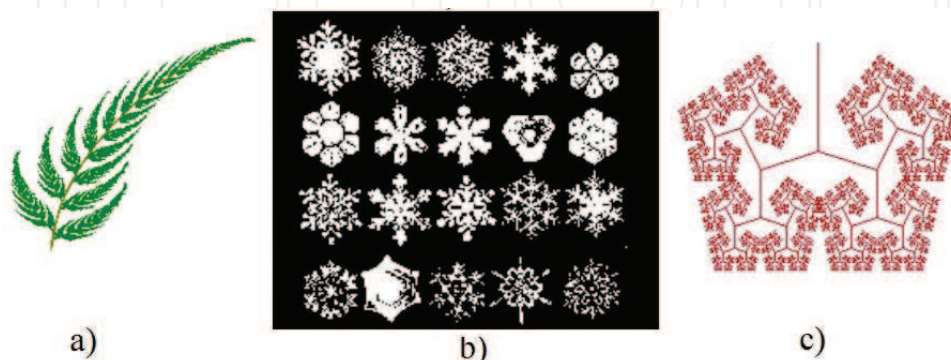


Figure 1. Fractal objects in nature: leaf of fern (a), the most popular—snowflakes (b) and human lungs formed by fractal canopies (c).

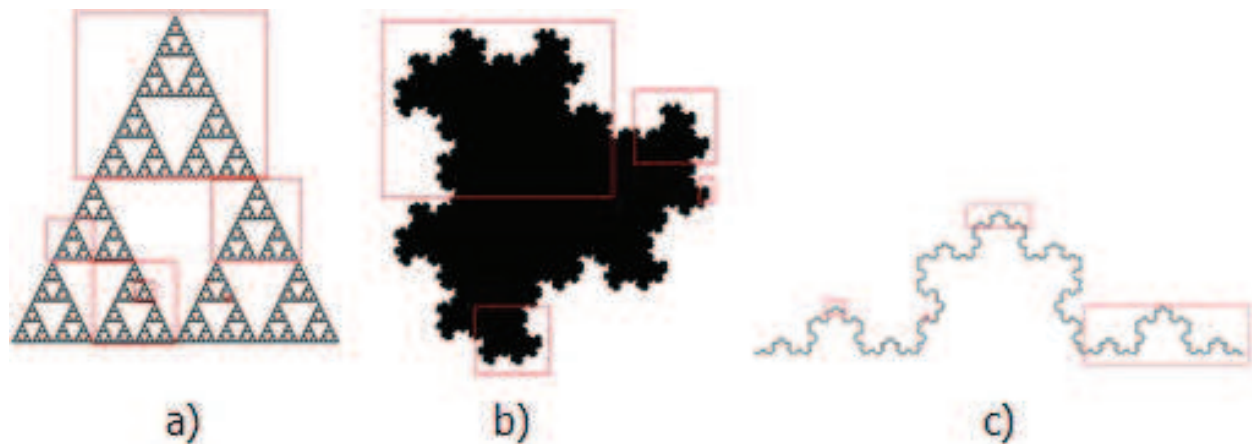


Figure 2. The self-similar components of different fractals: Sierpinski gasket (a), dragon (b) and Koch's curve (c).

1.2. Why use the antenna of fractal geometry?

Antennas are generally narrowband devices. Their properties depend on the size of the referenced to the wavelength. This means that for fixed antenna sizes, its parameters: power gain, input impedance, the radiation patterns, the side lobe level and distribution of surface currents will be continued strong changes when the operating frequency will change. Frequency dependency also means that the antenna should retain the minimum size in relation to the wavelength of operation, to work effectively. This means that for a given frequency, the antenna cannot be arbitrarily small, usually of the minimum size level of a quarter wavelengths.

These well-known rules for antenna engineers are being used for dozens of years in constructing the antennas of telecommunications systems. However, the dependence of the wavelength antenna size is still a problem in many systems where previously used antennas are not particularly useful. In this sense, the application of fractal geometry in the design of antennas and antenna arrays can help in dealing with the problems of designing antennas that meet the requirements of modern communication systems not found so far. The reason *why* the fractal design of antennas and MTM appears as an attractive way to make it is few-fold (**Figure 3**).

First, this is because you should expect each antenna similar to other, which is built with multiple copies of the same in different scales in size, to act in a similar way, for a few wavelengths. This means that the antenna should keep similar parameters of radiation for a few wavelengths.

Second, because the properties of the self-filling to an area of some fractals (fractal size) may allow small objects in the fractal shape to make better use of the small surrounding space. Fractal antenna and antenna arrays design derives from a mixture of two seemingly unconnected disciplines, namely, the theory of electromagnetism and geometry. From the first spiral and log-periodic antennas, developed in the early sixties of the 20th century by D.E. Isbell, R. DuHamelet and variants by P. Mayes [48] and from the works of Benoit Mandelbrot fractal geometry, the fractal antenna appears as a natural way to solve the problem of antenna working on multiple frequencies and antennas of reduced size.

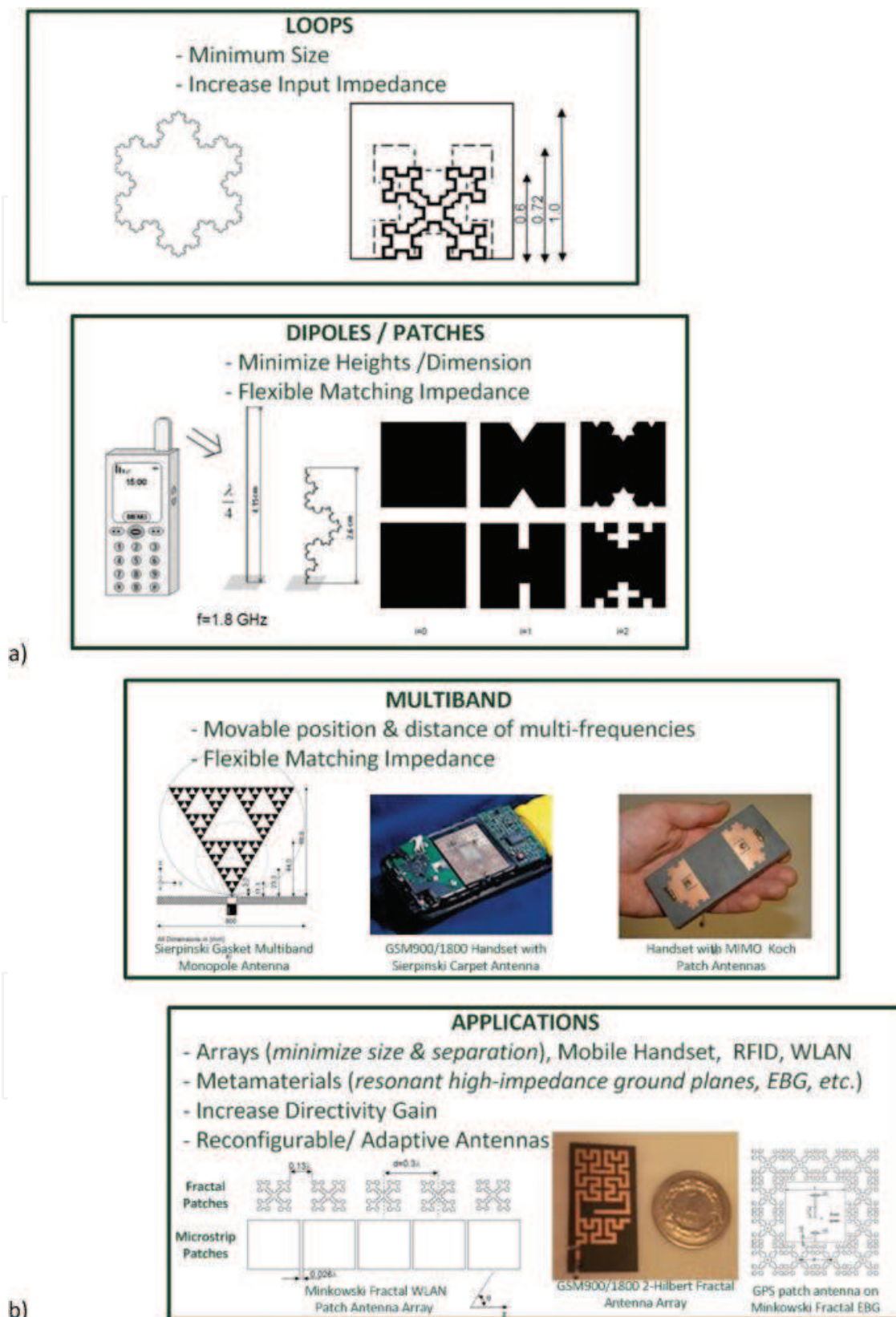


Figure 3. Fractal antennas (a) and the various fractal geometries, fall into few main categories: loops, dipoles, multiband fractal patches, antenna arrays, metamaterials (b).

1.3. How can you adopt fractal shapes in the design of antennas?

While Euclidean geometry is limited to points, lines, surfaces, and volumes, fractals include geometry, which come down between the two shapes. Therefore, a fractal can be a line, which is coming to the surface. The line can bend in such a way so as to effectively fill almost the entire surface. These properties of self-fill space lead to curves that are electrically very long but are located in a small space. This property can in effect lead to the miniaturization of antenna elements. In the previous section, it was mentioned that pre-fractals limit the complexity of fractal geometry, which is not recognized for specific applications. For antennas, it can mean that the curvatures, which are much smaller than the wavelength of the frequency range in use, can be dropped [11].

This causes the infinitely complex structure, which can be analysed only mathematically, not to be created physically. You can, however, show that the number of iterations required to achieve the benefits of miniaturization is limited to a few, before there will be the complexities difficult to distinguish in the so created structure. Not yet released many interesting works, which relate to the nascent field of the fractal electrodynamics.

Much of the pioneering work has been documented in Refs. [12, 13]. Most of them apply to mathematical foundations, as well as researches in the field of fractal antennas and/or EM wave reflection analysis of fractal surface. The area self-filling properties by the Hilbert fractal and related curves, e.g. the Peano fractal, make them attractive candidates for use in the design of antennas.

The Hilbert fractal self-filling properties were tested in Ref. [11] as an effective method to design a compact resonant antenna. The first four steps (iterations) of the construction of the Hilbert curve are shown in **Figure 4**.

The fractal structure of self-affine geometry [14] is shown in **Figure 4b**. It is constructed by scaling of the square, with a factor 3 in the horizontal direction, and a factor 2 in the vertical direction, creating six rectangles, out of which was removed in the top of the middle rectangle. This is the first iteration. The second iteration of this procedure is repeated for the remaining rectangles, and it can continue indefinitely. Such a way of generating fractal structures is defined by using the iterative function system (IFS).

1.4. The language of fractals

1.4.1. Iterated function system

A universal method to generate a variety of fractal structures is the iterative function system (IFS) introduced in Refs. [10, 15–22], that is based on the use of a series of affine transformations, w , defined by

$$w \begin{pmatrix} x \\ y \end{pmatrix} = \begin{pmatrix} a & b \\ c & d \end{pmatrix} \begin{pmatrix} x \\ y \end{pmatrix} + \begin{pmatrix} e \\ f \end{pmatrix} \quad (1)$$

where real number coefficients (a, b, c, d, e, f) are responsible for movement of fractal element in space: a, d —scaling, b, c —rotation by φ_1, φ_2 angles with respect to axis of coordinating system

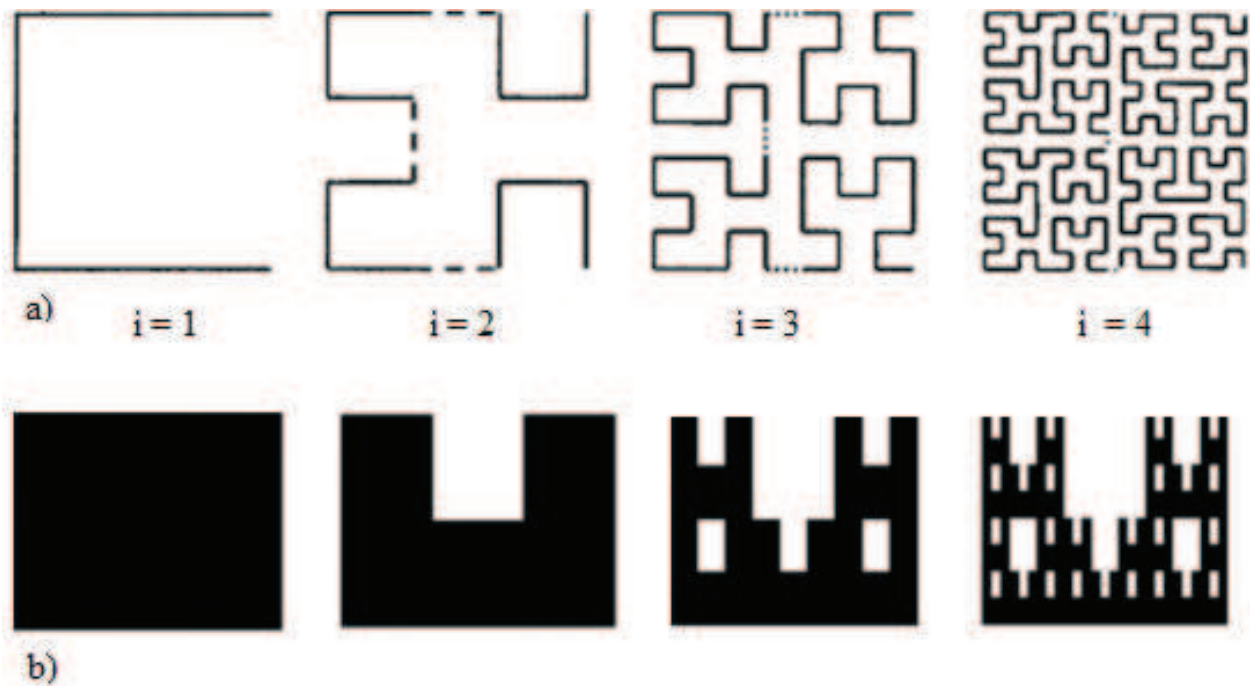


Figure 4. The four iterations of Hilbert fractal self-filing curve (a) and the self-affine fractal multiband antenna (b).

and e, f —linear translation by the vector (\mathbf{e}, \mathbf{f}) , respectively (see **Figure 5**). They are expressed as follows: $a = \delta_1 \cos \varphi_1$; $d = \delta_2 \cos \varphi_2$; $b = \delta_2 \sin \varphi_2$; $c = \delta_1 \sin \varphi_1$.

Suppose now that you should consider w_1, w_2, \dots, w_i as a system of linear affine transformations, and let A be the initial geometry. A new geometry you create by applying a series of transformations to the initial geometry and collecting the results of $w_1(A), w_2(A), \dots, w_i(A)$, which can be represented as follows:

$$W(A) = \cup_{i=1}^I w_i(A) \quad (2)$$

where W is known as the Hutchinson operator [15, 22].

The structure of the fractal can be obtained by using the operator W repeatedly, starting from the initial through geometry. For example, when the initial geometry represents A_0 , the next generation it gains as a result of

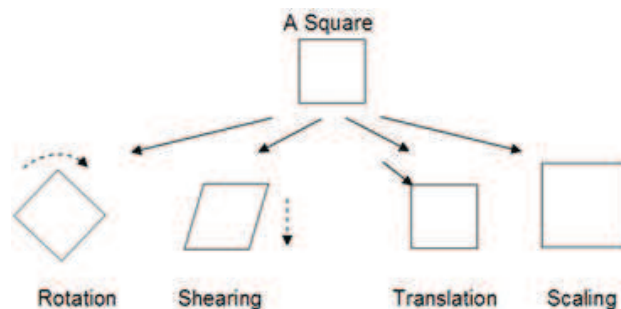


Figure 5. The affine transforms.

$$A_1 = W(A_0); A_2 = W(A_1); \dots; A_{k+1} = W(A_k) \quad (3)$$

Iterative system IFS generates sequences that converge to the final image A_∞ , and it is that the

$$W(A_\infty) = A_\infty \quad (4)$$

The result obtained is called an attractor of the IFS and represents a “fixed point” operator W . For the Koch fractal curve (**Figure 2c**), the affine transformation matrix has the form

$$w_q \begin{pmatrix} x \\ y \end{pmatrix} = \begin{pmatrix} \delta_{q1} \cos \theta_{q1} & -\delta_{q2} \sin \theta_{q2} \\ \delta_{q1} \sin \theta_{q1} & \delta_{q2} \cos \theta_{q2} \end{pmatrix} \begin{pmatrix} x \\ y \end{pmatrix} + \begin{pmatrix} t_{q1} \\ t_{q2} \end{pmatrix} \quad (5)$$

where the scaling factor is expressed as $\delta_q = (2 + 2 \cos \theta_q)^{-1}$, θ_{qi} is the inclination angle of the second subsection with respect to the first and t_{qi} is an element displacement on the plane.

Figure 6 illustrates the iterated function system procedure for generating the well-known Koch fractal curve.

In this case, the initial set, A_0 , is the line interval of unit length, i.e., $A_0 = \{x : x \in [0, 1]\}$; $\theta_q = 60^\circ$, and $\delta_q = \frac{1}{3}$.

The results of the four linear transformations are combined together to form the first iteration of the Koch's curve, described by A_1 . The second iteration, A_2 , of the Koch's curve can be obtained by applying to the A_1 same four affine transformations.

The Koch's curves of higher order are generated by repeating the iterative process, until you reach the desired resolution. The first four iterations of the Koch curve are shown in **Figure 6c**. **Table 1** shows the collection of the basic fractal structures, with particular importance for the construction of antennas for the low-frequency bands, multi-frequency operated as well as for the construction of metamaterials.

1.4.2. Self-affine sets

Self-affine sets form an important class of sets, which include self-similar sets as a particular case. An affine transformation $S : \mathfrak{R}^n \rightarrow \mathfrak{R}^n$ is as follow [15]:

$$w(x, y) = T(x, y) + t \quad (6)$$

where T is the affine transformation on \mathfrak{R}^n , which can be represented in $(n \times n)$ -matrix notation, and t is the vector in space \mathfrak{R}^n .

As you can see that the affine transformation is a combination of translation, rotation, dilation and reflection (**Figure 4b**). In particular, w could convert the sphere to an ellipsoid, squares to parallelograms, etc. Unlike the similarity, affine transformations are accomplished with different coefficients in different directions.

If w_1, \dots, w_m are self-affine construction on \mathfrak{R}^n , so it is a unique, unchanging set of F for the w_i is referred to as the self-affine set of equations. In **Figure 5**, w_1 , w_2 and w_3 are defined as

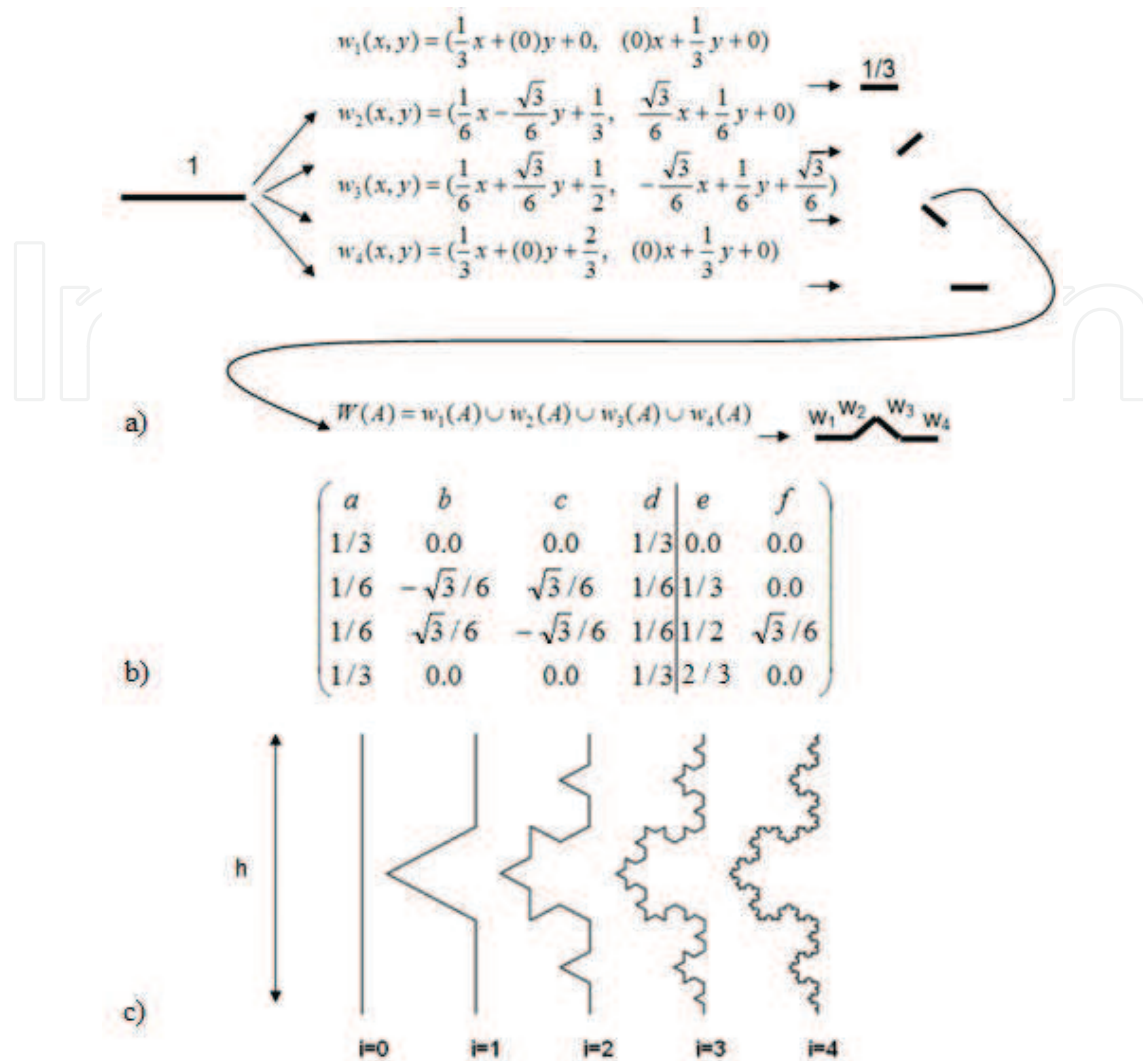


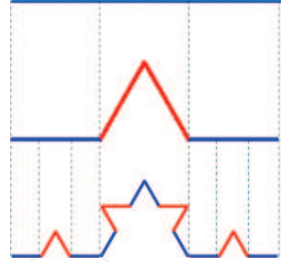
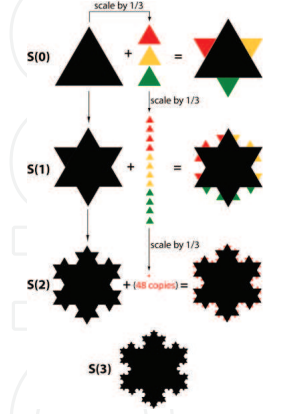
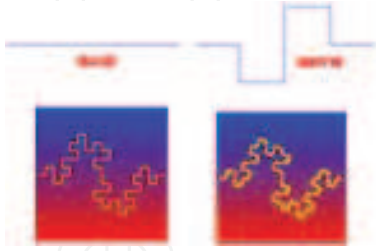
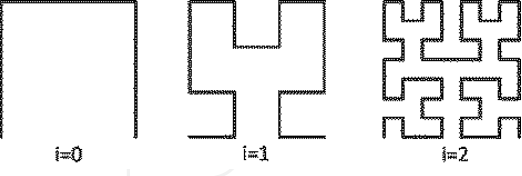
Figure 6. The IFS (a), the affine transformation matrix (b) and the first four iteration steps of construction (c) of the Koch fractal curve.

transformations that map the section into three equal sections, obviously. It is natural, therefore, to search for the description for size self-affine transformations, which will serve as the generalization of the formula for systems and geometries with similar affine transformations.

We hope that the dimension depends on the formula of affine transformation set in a relatively simple way, easily presented to the matrix and/or the vectors that represent transformation. Unfortunately, the situation is more complicated. If the affine transform change continuously, the dimensions of the set of self-affine do not need to change continuously. Such intermittent behaviour becomes more difficult for the more complex affine transformation; therefore, it may be difficult to obtain a general expression in the form of affine sets.

1.4.3. The fractal dimension

In general, we can imagine objects that have a zero dimension, 0D (points), 1D (lines), 2D (plane) and 3D (solid). We feel comfortable with the objects of such dimensions. We create a 3D

Fractal type	Similarity dimension	Iterated function system	Sketch of iterated structure
Koch curve	1.26186	$w_1(x, y) = [\frac{1}{3}x; \frac{1}{3}y]$ $w_2(x, y) = [\frac{1}{6}x - \frac{\sqrt{3}}{6}y + \frac{1}{3}; \frac{\sqrt{3}}{6}x + \frac{1}{6}y]$ $w_3(x, y) = [\frac{1}{6}x + \frac{\sqrt{3}}{6}y + \frac{1}{2}; -\frac{\sqrt{3}}{6}x + \frac{1}{6}y + \frac{\sqrt{3}}{6}]$ $w_4(x, y) = [\frac{1}{3}x + \frac{2}{3}; \frac{1}{3}y]$	
Koch snowflake	2	$w_1(x, y) = [\frac{1}{2}x - \frac{\sqrt{3}}{6}y; \frac{\sqrt{3}}{6}x + \frac{1}{2}y]$ $w_2(x, y) = [\frac{1}{3}x + \frac{1}{\sqrt{3}}; \frac{1}{3}y + \frac{1}{3}]$ $w_3(x, y) = [\frac{1}{3}x; \frac{1}{3}y + \frac{2}{3}]; w_4(x, y) = [\frac{1}{3}x - \frac{1}{\sqrt{3}}; \frac{1}{3}y + \frac{1}{3}]$ $w_5(x, y) = [\frac{1}{3}x - \frac{1}{\sqrt{3}}; \frac{1}{3}y - \frac{1}{3}]$ $w_6(x, y) = [\frac{1}{3}x; \frac{1}{3}y - \frac{2}{3}]$ $w_7(x, y) = [\frac{1}{3}x + \frac{1}{\sqrt{3}}; \frac{1}{3}y - \frac{1}{3}]$	
Minkowski curve	1.5	$w_1(x, y) = [\frac{1}{4}x; \frac{1}{4}y]; w_2(x, y) = [-\frac{1}{4}y + \frac{1}{4}; \frac{1}{4}x]$ $w_3(x, y) = [\frac{1}{4}x + \frac{1}{4}; \frac{1}{4}y + \frac{1}{4}]$ $w_4(x, y) = [-\frac{1}{4}y + \frac{1}{2}; \frac{1}{4}x + \frac{1}{4}]$ $w_5(x, y) = [-\frac{1}{4}y + \frac{1}{2}; \frac{1}{4}x]; w_6(x, y) = [\frac{1}{4}x + \frac{1}{2}; \frac{1}{4}y - \frac{1}{4}]$ $w_7(x, y) = [-\frac{1}{4}y + \frac{3}{4}; \frac{1}{4}x - \frac{1}{4}]; w_8(x, y) = [\frac{1}{4}x + \frac{3}{4}; \frac{1}{4}y]$	
Hilbert curve	1.2619	$w_1(x, y) = [\frac{1}{2}y - \frac{1}{2}; -\frac{1}{2}x - \frac{1}{2}]$ $w_2(x, y) = [\frac{1}{2}x - \frac{1}{2}; \frac{1}{2}y + \frac{1}{2}]$ $w_3(x, y) = [\frac{1}{2}x + \frac{1}{2}; \frac{1}{2}y + \frac{1}{2}]; w_4(x, y) = [-\frac{1}{2}y - \frac{1}{2}; \frac{1}{2}x - \frac{1}{2}]$	


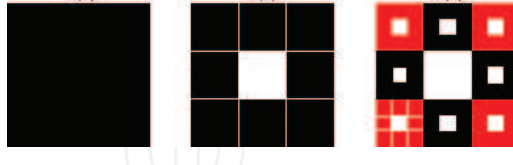

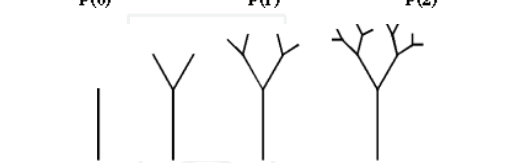

Fractal type	Similarity dimension	Iterated function system	Sketch of iterated structure
Sierpinski gasket	1.58496	$w_1(x, y) = [\frac{1}{2}x; \frac{1}{2}y]; w_2(x, y) = [\frac{1}{2}x + \frac{1}{2}; \frac{1}{2}y]$ $w_3(x, y) = [\frac{1}{2}x + \frac{1}{4}; \frac{1}{2}y + \frac{\sqrt{3}}{4}]$	
Sierpinski carpet	1.89279	$w_1(x, y) = [\frac{1}{3}x; \frac{1}{3}y]; w_2(x, y) = [\frac{1}{3}x; \frac{1}{3}y + \frac{1}{3}]$ $w_3(x, y) = [\frac{1}{3}x; \frac{1}{3}y + \frac{2}{3}]; w_4(x, y) = [\frac{1}{3}x + \frac{1}{3}; \frac{1}{3}y]$ $w_5(x, y) = [\frac{1}{3}x + \frac{1}{3}; \frac{1}{3}y + \frac{2}{3}]$ $w_6(x, y) = [\frac{1}{3}x + \frac{2}{3}; \frac{1}{3}y]; w_7(x, y) = [\frac{1}{3}x + \frac{2}{3}; \frac{1}{3}y + \frac{1}{3}]$ $w_8(x, y) = [\frac{1}{3}x + \frac{2}{3}; \frac{1}{3}y + \frac{2}{3}]$	
Sierpinski pentagon	1.67228	$w_1(x, y) = [0.382x; 0.382y]$ $w_2(x, y) = [0.382x + 0.618; 0.382y]$ $w_3(x, y) = [0.382x + 0.809; 0.382y + 0.588]$ $w_4(x, y) = [0.382x + 0.309; 0.382y + 0.951]$ $w_5(x, y) = [0.382x - 0.191; 0.382y + 0.588]$	
Fractal Tree	1.5849	$w_1(x, y) = [\frac{1}{3}x; \frac{1}{3}y + 2]; w_2(x, y) = [\frac{1}{3}x - \frac{4}{3}; \frac{1}{3}y + 2]$ $w_3(x, y) = [\frac{1}{3}x + \frac{4}{3}; \frac{1}{3}y + 2]$	
Cantor Set	0.63092	$w_1(x, y) = [\frac{1}{3}x; \frac{1}{3}y - W]$ $w_2(x, y) = [\frac{1}{3}x + \frac{2}{3}; \frac{1}{3}y - W]$	

Table 1. Collection of the fractal structures useful in construction of antenna and metamaterials.

image of our world by combining 2D images from each of our eyes. You can also imagine multidimensional objects, that is, 4D, 5D, 6D. And, what about objects which have non-integer dimensions, such as 2.12 D, 3.79 D or 36.91232 ... (D)? Classical methods of geometry and calculus are not suitable for studying fractals, and that is why we need alternative techniques.

There are many definitions of fractal dimensions [22], many of them are evaluated in Ref. [15] that include: similarity dimension, DS ; the division dimension, DD ; the Hausdorff dimension, DH ; the boxing counting dimension, DB ; the correlation dimension, DC ; the information dimension, DI ; the point wise dimension, DP ; the averaged point wise dimension, DA ; and the Lyapunov dimension, DL . The last seven dimensions listed are particularly useful in identifying the fractal structures in the form of strange attractors, related to the chaotic dynamics.

So, the main tool for the description of fractal geometry is a dimension, in many forms. In a large simplification, the dimension determines how much space has been filled. This is a measure of how many are exposed irregularities when we look at in a very small scale. The dimension contains a lot of information about the geometric properties of the fractal structure.

In the classification of fractals, one of the most important is the Hausdorff dimension [22]. In fact, Mandelbrot suggested that fractal can be defined as an object that has a Hausdorff dimension, exceeding its topological dimension. A complete mathematical description of Hausdorff dimension is beyond the scope of this text [15]. In addition, the Hausdorff dimension is not particularly useful for an engineer or a scientist wanting to evaluate the fractal object, because it is virtually impossible to designate the actual data.

The Hausdorff dimension, for example, and the box counting dimension can be defined for any sets and you can show that they are equal to the similarity dimension. We will focus on the use of the similarity dimension, DS , to characterize the properties of regular fractals. The dimension DS is a key parameter for describing the structure of the self-similar fractal and is defined by the segmenting of the volume covering the fractal, on cubes of side δ . We assume that at least one of the cubes will contain the described fractal

$$N(\delta) \sim \delta^{-D} \quad (7)$$

The concept of dimension is closely associated with scaling. Consider lines, surfaces, and solids, divided by self-similar shorter segment, smaller surfaces and little volumes, with a side δ . For simplicity, assume that the length L , the area A and the volume V are equal to unity. First, consider the line, divided into N smaller segments, each with a length of δ . In this case δ is the factor scale that means $\delta/L = \delta$ with line of a unity length of N equal segments, scaled by $\delta = 1/N$.

Now consider the unit area. If we divide it into N segments, each with an area δ^2 , because $A = N\delta^2 = 1$, i.e. per unit area consists of N identical scaled by $\delta = 1/N^{1/2}$. Using similar reasoning, the unit for volume $V = n \delta^3 = 1$, which is the unit of volume consists of N identical cubes scaled by $\delta = 1/N^{1/3}$ self-similar parts. Comparing the above expressions, we see that the exponent δ in each case is a measure of the similarity of the object. We can generally describe it as

$$N \delta^{DS} = 1 \quad (8)$$

In logarithmic measure, it leads to an expression,

$$DS = \frac{\log(N)}{\log(\frac{1}{\delta})} \quad (9)$$

Note that here the letter “*S*” denotes the similarity dimension. The above expression has been derived using familiar objects, which have the same integer Euclidean, topological and similarity dimensions, i.e. a straight line, planar surface and solid object, where $DE = DS = DT$. However, Eq. (9) may also be used to produce dimension estimates of fractal objects where DS is non-integer. The DS dimensions of all representative fractals are introduced in **Table 1**.

2. Useful fractal geometry in antenna engineering

After reviewing the properties of fractal geometry, you might want to explain what benefits you can get with such geometry used in the construction of antennas. Fractals are abstract objects, which cannot be implemented physically. You can apply some simplification in approach to an ideal of fractals, which will allow you to use them in the construction of antennas. Such simplified geometries are called pre-fractals or truncated fractals.

Configurations, consisting of many triangles or multilevel meandered structures, that are close to the fractal shapes and have some advantages, which in theory can be obtained only as a result of mathematical abstraction, can be used as antennas. Generally, the term “fractal antenna technology” is used to describe these antenna engineering techniques, which are based on mathematical concepts, enabling the creation of a new generation of antennas, which, even in the mid-1980s, were often regarded as impossible to achieve.

As a result of the works carried out so far, you can point to the benefits of using the fractal antenna technology: (1) self-similarity is useful in the design of the antenna working on multiple frequencies, for example, the Sierpinski triangle, fractal tree and the Cantor set; (2) self-filling reduces the overall dimension and is useful for the design of small antennas, such as monopoles/loops/microstrip patches of Hilbert, Peano, Minkowski, Koch fractal shapes; (3) mass fractals and boundary fractals are used in the construction of antenna of high directivity and low sidelobes level.

Probably the earliest publication in which the term fractal radiating element, fractal antenna for the determination of elements made of crooked wires appeared was released in May 1994 [23].

2.1. Fractal dipole antenna

An interesting study of the space-filling properties of fractal antennas is to investigate fractal dipole antennas. Three types of Koch fractals were compared as dipoles. They are depicted in **Figure 6c** and **Table 1**, for the first stages of growth. The Koch fractal dipole is shown in **Figure 7**.

The output structure for construction of fractal Koch [24] and fractal tree [25] was dipole antenna of height h . As previously calculated (**Table 1**), Koch fractal has a fractal (similarity) size of $DS = 1.2619$. Fractal tree is similar to a real tree, in the sense that at the top each branch is divided into more branches. In the tree, flat (two-dimensional) each of the three branches is

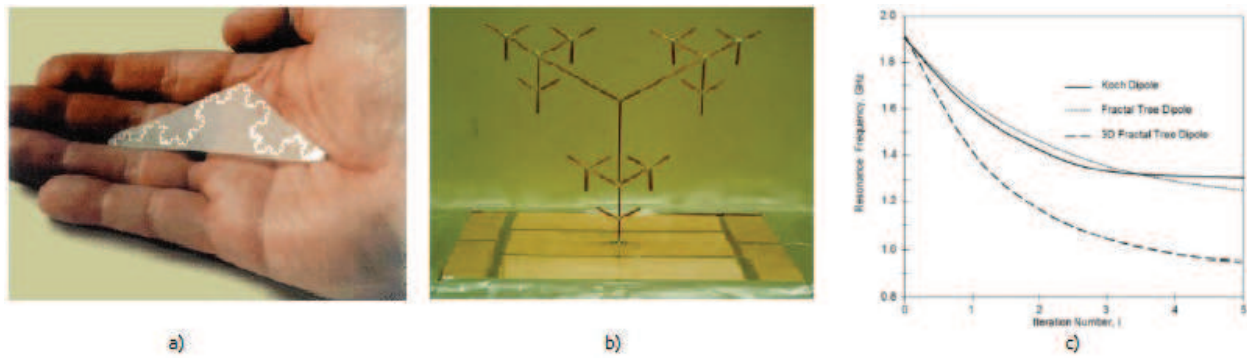


Figure 7. Koch fractal dipole printed on microwave laminate (a), wire fractal tree (b) and resonant frequencies of Koch, two-dimensional and three-dimensional trees fractals versus iteration (c).

divided into two sections. The length of each branch remains the same, in this way, going from the base of the tree to the top of the branches have the same length as the initiator. Fractal dimension (the similarity) is equal to $DS = 1.395$ for flat tree and 1.5849 for the three-dimensional tree.

Decrease in the resonance frequency has the same effect as the miniaturization of antenna at a constant frequency. The same can be said about the flat antenna structures. The use of non-planar structures, 3-D, increases this effect.

As you can see from the research, the benefits of the application of fractal for miniaturization antennas are already achieved by the first few iterations. By observing the resonance frequency of the antenna, it is also very interesting to look at the quality factor Q of these antennas [15, 26]. It can be observed if due to fact that fractal wire antenna fills the space more effectively than linear dipole, it has lower Q -factor. Quality factor is reduced for greater number of iterations, what can be expected. Any increase in the generation of iteration brings the geometry of fractal away from the linear one-dimensional dipole and closer to the ideal fractal.

As mentioned many times before, an important feature of much fractal geometry is the self-filling. The size of the antenna is a critical parameter, because the electromagnetic properties depend on the antenna dimensions related to the wavelength (λ). In many applications, the amount of space occupied by an antenna is a factor limitations, therefore, may not be comparable to the wavelength, but less, that are called the small antennas. It is said that the antenna is electrically small, when its largest dimension is smaller than the diameter of the sphere of which the radius r is of specified dependency $r = \lambda/2\pi$ [15]. Wheeler and Chu were the first who showed the fundamental limitations of such antennas. Hilbert, Koch, Peano fractals are especially useful in the design of small antennas. The purpose of this section is to present characteristics of miniature microstrip (printed) antennas in the shape of a Hilbert curves and Koch patches.

2.2. Fractal patch antennas

Fractals can be used for miniaturization of surface antenna, as well as linear elements. Applies the same concepts in order to increase the electrical dimensions of flat radiating element as wire were [15–21, 26, 27]. Flat antenna can be seen, as a microstrip line with extended

transverse dimensions. Therefore, if the electric current is forced to flow along the meandered fractal path instead of a simple Euclidean path, the area required for the placement of resonant transmission line can be greatly reduced. This technique has been applied to the design of, so-called microstrip antennas of different shapes of patches of fractal geometry, which are fabricated (printed) by means of photo etching technology or in the fast laser prototyping processes.

One of the fractal structures was discovered in 1916 by Polish mathematician Waclaw Sierpiński. So called, Sierpinski gasket applied to the construction of the antenna has the properties of multi-frequency operations, due to the fact that it is made up of similar triangles, in each of the roof in the heights scaled with the factor δ . This design was first proposed by Puente et al. [28] (**Figure 8**).

From the point of view of antenna engineering, interpretation shown in **Figure 8a** is such that the dark areas of the triangle represent the conductive metallic surfaces, white areas of the triangle represent surfaces where metal has been removed. With few exceptions (notably log-periodic aerials), typically we use a single antenna for our system (frequency) as shown in **Figure 8b**. So, in this case, we have three antennas in one compact configuration. The geometry of fractal antenna in the form of a Sierpinski gasket is completely determined by four parameters: the height h of the triangle, the countersink angle α , the number of iterations I , and by the

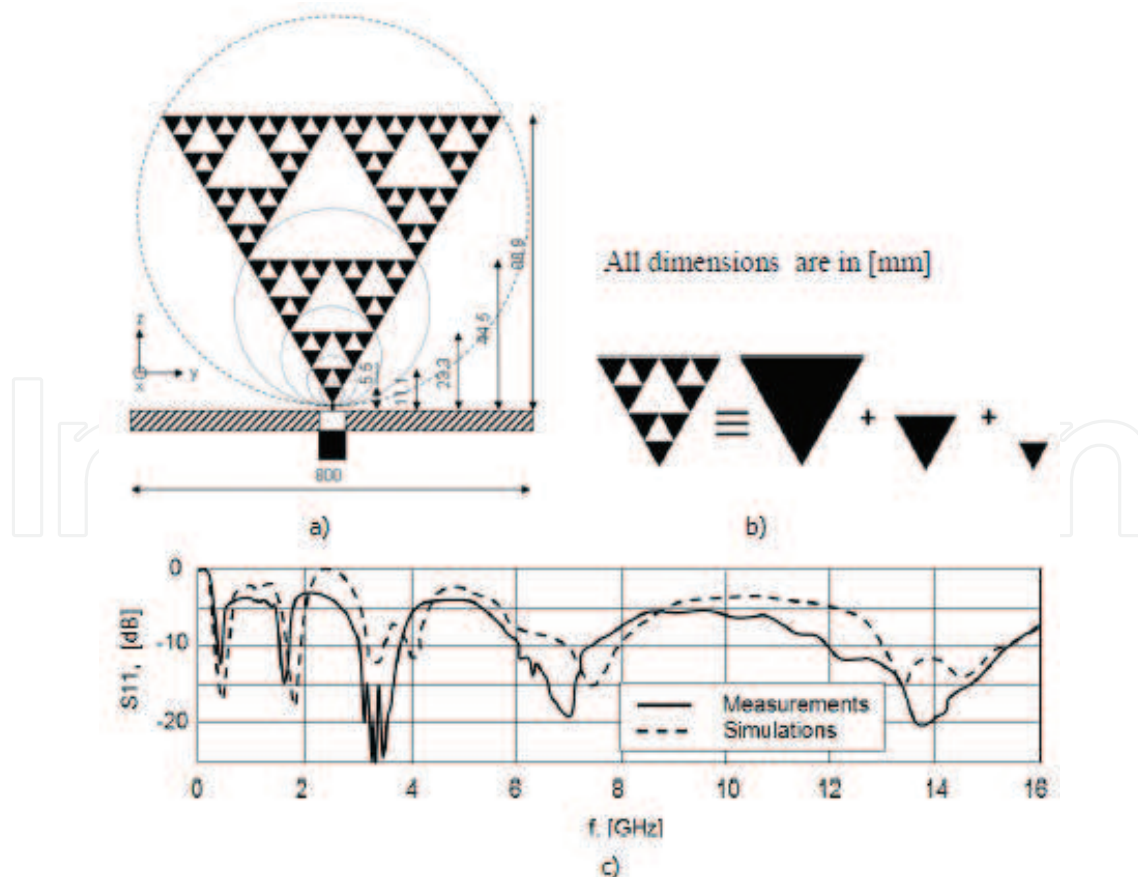


Figure 8. Sierpinski fractal gasket triangle of fifth-iteration as monopole antenna (a), second-iteration Sierpinski triangle as equivalent antenna to an array of three triangles (b) and input reflection coefficient of antenna (a) versus frequency (c).

scaling factor ($\delta = h_i/h_{i+1}$, where h_i is the height of triangle). As it was described in Ref. [20], the Sierpinski monopole behaves like the antenna of logarithmic-periodic geometry [16, 19, 29] (**Figure 8c**), with the each next resonant frequencies separated by the distant relative but reversed to self-similarity scale factor $\delta = 2$. The antenna has similar parameters for the next resonant frequency, with a moderate bandwidth $BW = 21\%$ [15–17, 28, 29, 48].

$$f_{ri} = 0.3 \cos\left(\frac{\alpha}{2}\right) \sqrt{\frac{2.5}{\epsilon_{\text{reff}}}} \frac{c}{h} \delta^i \quad (10)$$

where c is the speed of light in vacuum, h is the height of the largest gasket, δ is the log period scaling factor, i is a natural number of iterations, and ϵ_{reff} is the effective permittivity of the antenna substrate.

Figure 9 shows the new flat IFA antenna (inverted-F-antenna) made in the form of the Hilbert fractal curve for use in handset of mobile cellular phone GSM 900/1800 system. Such geometry of the antenna effectively increases the length of the path for the electrical current comparably to a simple antenna IFA, occupying the same surface. Such solution allows significant miniaturization of the antenna. To support the two frequency bands of GSM, two antenna elements are designed in the shape of a fractal Hilbert.

Antenna, consisting of two elements in the form of a Hilbert pre-fractal, as shown in **Figure 9**, is designed for GSM 900/1800 mobile system handset [9]. The smaller element, near the power point, works on a higher frequency of 1.8 GHz, while the bigger one at $f = 900$ MHz. Each element has been built in the form of a Hilbert curve of second iteration $i = 2$. The antenna was fabricated on one-side metalized microwave laminate of type DUROID-5880 ($h_s = 0.125$ mm, $\epsilon_{rr} = 2.2$, $\tan\delta = 0.009$) and placed on the foam, Rochacell 51

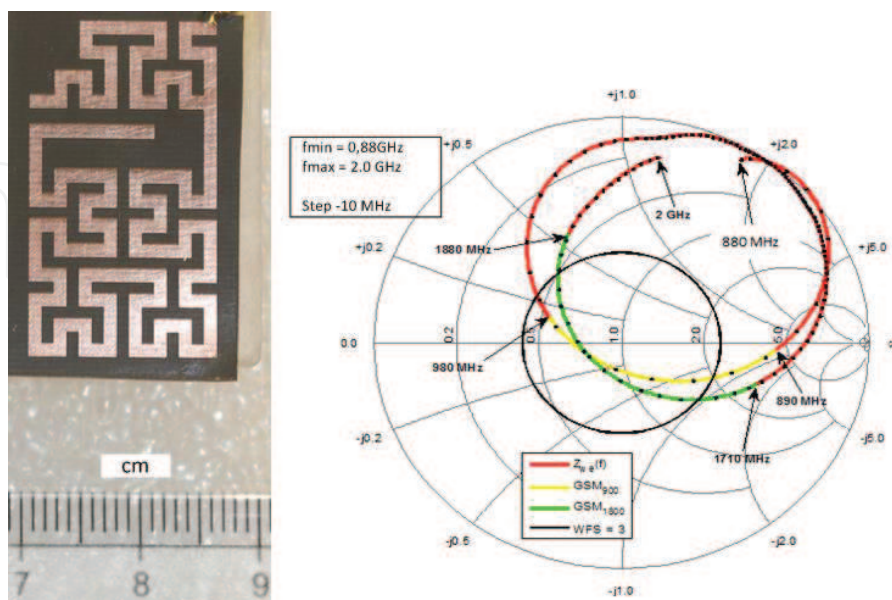


Figure 9. Photo of miniaturized Hilbert fractal PIFA antenna (a) and input impedance plot on Smith Chart (b).

IG/A ($h_f = 9$ mm, $\varepsilon_{rr} = 1.071$, $\tan\delta = 0.0031$). This design is about 50% (~ 4.3 cm³) of the volume occupied by the conventional microstrip planar inverted-F, PIFA antenna.

Another microstrip patch antenna with edges in the shape of a Koch pre-fractal [30] is shown in **Figure 10**. It was designed for the handset terminal, smartphone, cooperating with several mobile communication systems: GSM1800, UMTS and HiperLAN2. Application of PIFA antenna in conjunction with the fractal geometry reduces antenna size by 62% compared to the conventional PIFA.

Two identical PIFA antennas, in the form of Koch pre-fractal (as former one), are placed above the screen of finite sizes (100×45 mm²—the typical size of a smartphone) have been applied for MIMO (Multiple Input Multiple Output) system.

The Sierpinski fractal carpet (**Figure 10b**) was used by the Spanish company FRACTUS, to build the build-in antenna of a mobile cellular system GSM 900/1800 handset.

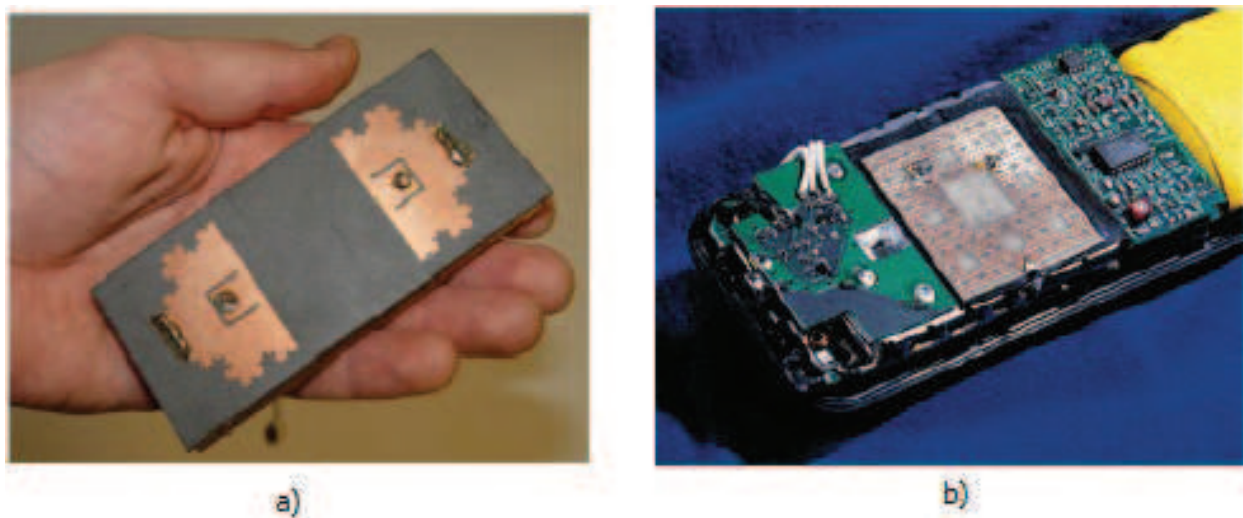


Figure 10. Photos of the microstrip patches of Koch fractal double-PIFA (a) and Sierpinski carpet (b) antennas.

3. Metamaterials in electromagnetics applications

3.1. Introduction

Basic research and applications of electromagnetism have undergone different phases of development, keeping pace with the general socio-technology growth [3]. Currently, there is a huge demand for small antennas for mobile communication systems [31]. In the microwave frequency range, It is tried to solve the problem by the use of artificial dielectrics and or magnetic materials, so-called metamaterials, MTMs. They have been used in place of traditional one as surrounding environment, e.g. the substrates or ground planes to build antennas, filters and other microwave devices. The MTMs are also used, as energy absorbers of electromagnetic waves in order to eliminate the effects of surface currents, which can cause unwanted EM-coupling between nearly situated elements or produce the reflected signals (echoes) in radar applications.

We distinguish two main categories of metamaterials: (1) SNGs are such one, which are characterized by single-negative ($-\epsilon$ or $-\mu$) and DNG the double-negative ($-\epsilon$ and $-\mu$) material parameters, built with the cells of small sizes ($\sim \lambda/10$); (2) EBGs are so-called electromagnetic bandgap materials, and FSSs are the frequency selective materials, where the periodic structure is built out of cells of size comparable with the wavelength (typical $\lambda/2$).

The MTMs completely revolutionized the construction technologies of small microwave components such as antennas, filters, and others that provide high directivity (antenna) attenuation (filters) in a wide range of frequencies that are comparable to those they had previously used in microwave devices of much larger sizes.

3.2. Electromagnetic environment of negative material parameters

Electromagnetic materials in nature play a major role in operation of the instruments operating on the basis of the phenomena of electricity and magnetism, such as capacitors, inductors, resonant circuits and, in general, the physics of propagation of EM waves. The discovery of artificially made materials with unusual properties such as negative electrical permittivity and/or permeability, causing the occurrence of negative refractive index, negative propagation of EM waves and the inverse Doppler effect [3, 33–37] changed the way of thinking of scientists and engineers.

It is well known that the reaction of the system for the presence of the electromagnetic field depends to a large extent on the properties of the materials used and the parameters of the environment in which they occur. Therefore, the behaviour of the material (environment), in the presence of the electromagnetic field, depends on the macroscopic material parameters: permittivity ϵ , permeability μ and conductivity σ . **Figure 11** shows the classification of materials on the basis of the parameters ϵ and μ .

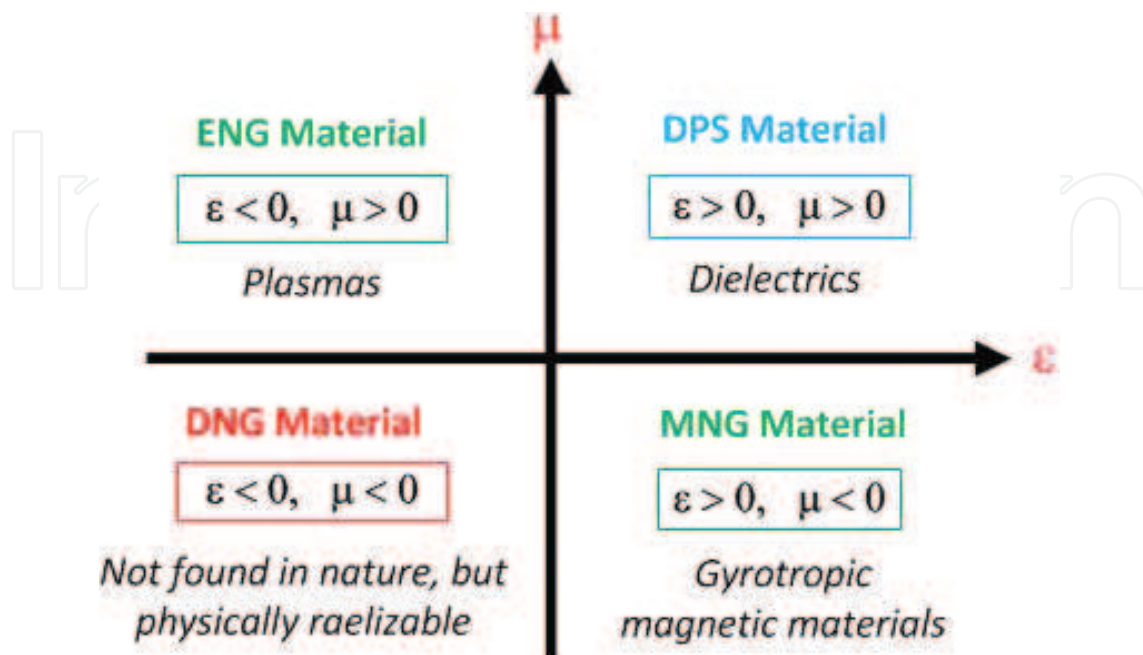


Figure 11. Material classifications.

Concept of metamaterial (MTM) technology appeared in the 1990s, with the work of about macroscopic composites of synthetic cells, periodic over the matter [2]. However, the initial attempts to use “artificial” materials were initiated in the end of nineteenth century in 1898 by Jagadis Chunder Bose carried out by his experiment with coiled structures [38]. Lindman was next in the artificial media explorers, who researched the artificial chiral media in 1914 [39].

In the last 20 years since the end period of twentieth century, an increased interest in MTM technologies has been observed. This involves researches on super lens, applications in telecommunications, including antennas and transmission lines [40], and nowadays in the direction of improving the parameters of microwave devices, which will then satisfy the electromagnetic compatibility of communication systems [41]. As mentioned previously, MTM is the composite of macroscopic cells of periodically or non-periodically distributed all around structure, whose parameters depend on the cells architecture and the chemical composition [42]. MTMs are formed through the introduction of integration (e.g. molecules) in the structure of the material of the dielectric substrates. These inclusions change the electromagnetic properties of dielectric material of interest. In this work, different MTM patterns as fractal cells, and CLL cells, are applied. Almost all bulk MTMs used at the present state of art are based on cell structures that consist of a dense array of thin wires DWA, a ring resonator—RR (Ring Resonator) or CLL (Capacitively Loaded Loop) in SRR (Split Ring resonator) or CSRR (Complementary Split Ring Resonator) configuration topologies. They are oriented according to the wave direction.

V. G. Veselago suggested a novel aspect at this new kind of materials [3]. Theoretical foundation of the occurrence of the “*electromagnetic materials that exhibit both negative values for ϵ and μ* ” was published in 1968 [32]. It describes some of the properties of these materials, such as (1) a negative refractive index, (2) phase reverse, (3) left-handed triad, (4) reversed the effect of the Vavilov-Cerenkov, (5) inverted Doppler effect, (6) anisotropy frequency dispersion and so on. Using them, it means the MTM, to build electromagnetic instruments makes the lens completely flat, and the waves on the border of media with such materials are reflected in the same direction where they come from. Nowadays a number of names for the MTM with negative permittivity and negative permeability have been used such as (1) LH—left-handed media; (2) NRI—a negative refraction index media; (3) the BWM backward wave media; and (4) DNG MTM double negative-MTM.

3.3. Dipoles and loops as the building cells of metamaterial

The structures proposed in Ref. [32] do not exist in nature; therefore, try to create them artificially in the laboratory. The MTMs are created in the form of small cells as inclusions or homogeneities embedded in the host medium. They could also be attached or embedded on the surface of the host substrate. One of the most widely used structures MTM are arrays of densely spaced elementary electrical dipoles, in the form of thin wires [43] (**Figure 12**).

If the operating frequency is lower than the cut-off frequency of an array (“plasma frequency”), the equivalent effective permittivity (1) is negative (ENG). When a lattice constant a is much smaller than a wavelength ($a \ll \lambda$), the wire array can be thought as a continuous plasma like material described by an equivalent macroscopic ϵ —relative permittivity [4]:

$$\epsilon_{\text{reff},z} = \epsilon'_{\text{reff},z} - j\epsilon''_{\text{reff},z} = 1 - \frac{f_p^2}{f^2 - j\gamma f} \quad (11)$$

where, $\epsilon_{\text{reff},z}$ denotes the effective relative permittivity in the z-direction, f and f_p represent the signal frequency and the cut-off-frequency of the array, respectively, whereas γ is a factor that represents losses.

Eq. (11) applies only if the propagation takes place in transversal (x-y) plane.

The plasma frequency generally depends on the geometry of the system (a lattice constant, wire radius). The relative ϵ in the transversal directions (x and y) is always positive and, in a case of thin wires, is approximately equal to that of vacuum ($\epsilon_{\text{ref } x,y} \cong 1$). Permittivity is positive above the plasma frequency (EPS). However, if the frequency is only slightly higher than the plasma frequency, the structure will support the propagation of waves with a wavelength much longer than the length of the wave in free space, because of the relative permittivity that takes very small positive values ($\epsilon_r \ll 1$). In this region, the structure behaves like a low-loss of epsilon-near-zero, ENZ MTM.

Such MTMs give rise to the phenomena of ultra-reflection and spatial filtering, which can be used to increase the directivity of simple antennas. Currently, the MTMs are implemented in the form of an array of metallization properly oriented in space, which is therefore internally homogeneous and microscopic. On the other hand, the size of the metallization and the distance between them are very small compared to the wavelength (electrically small). Relying on the theory of effective media, it is reasonable, therefore, to seek the bulk properties, in this case, the bulk permittivity and permeability that characterize the macroscopic behaviour of the medium.

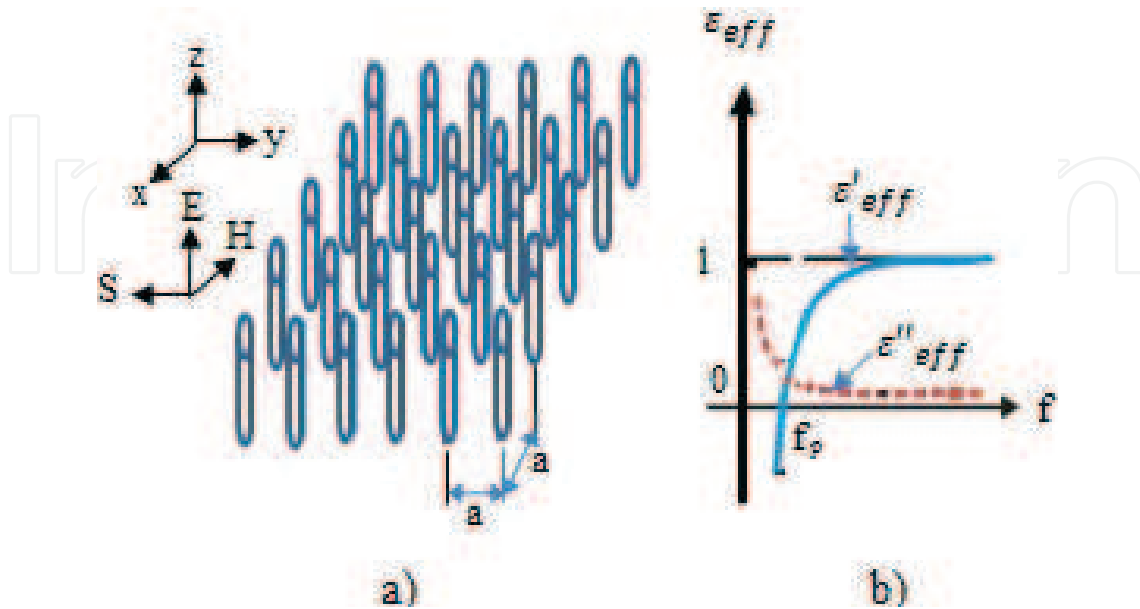


Figure 12. An array of dipoles in the form of thin-wires-based MTM (a) and effective permittivity of such MTM (b).

Since the first theoretical introduction in Ref. [6], an array of SRR inclusions (**Figure 13a**) has been widely used for the synthesis of MNG metamaterials [4].

A SSR can be thought of as a small, CLL-loaded antenna [4]. If the antenna is working just above the resonance frequency, local distributed magnetic field will be almost in the opposite phase relative to the incident field. Therefore, the resulting local magnetic field will be smaller than the incident field. It leads to a negative magnetic polarity and negative effective permeability of the resulting metamaterial. It has been shown that the effective permeability of such metamaterials can be specified on the basis of an analysis of loop antenna system used in the cells that make up the MTM [4].

$$\mu_{\text{eff}} = \mu'_{\text{eff}} - j\mu''_{\text{eff}} = 1 - \frac{f_{\text{mp}}^2 - f_0^2}{f^2 - f_0^2 - j\gamma f} \quad (12)$$

where f is the frequency of the signal, f_{mp} denotes the frequency in lossless case when $\mu_{\text{eff}} = 0$ ("magnetic plasma frequency"), f_0 is the frequency at which μ_{eff} diverges (the resonant frequency of SRR) and γ represents the losses.

Eq. (12) describes the simplified SRR model that does not take into account the minor electrical polarization [44] and some small bi-anisotropic effects [45], which obviously influences the effective permeability. The SRR is treated as a purely magnetic particle.

Figure 13b shows the dependence of the effective permeability μ_{eff} as a function of frequency. The frequencies of the f_{mp} and f_0 depend on architecture of SSR distribution, as well as its geometric parameters (internal and external radiuses and the width of the slits) [44]).

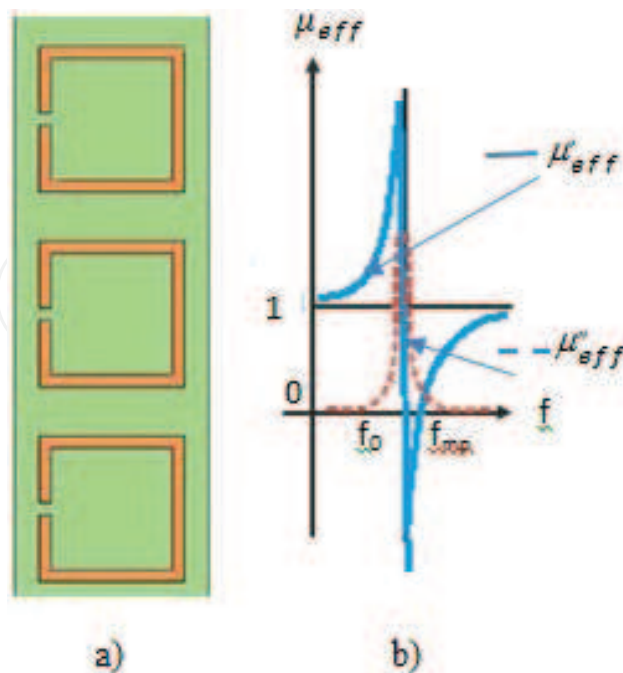


Figure 13. An array of SRRs (a) and effective permeability of array (b).

A general SRR-array-based MNG MTM can be described by a 2×2 uniaxial permeability tensor:

$$\bar{\mu} = \mu_0 \begin{bmatrix} \mu_{tr} & 0 \\ 0 & \mu_{lr} \end{bmatrix} = \mu_0(\bar{\mu}'_r - j\bar{\mu}''_r) = \mu_0\bar{\mu}_r \quad (13)$$

where μ_0 is the absolute permeability and μ_{tr} and μ_{lr} are the relative permeability in the transversal (x) and longitudinal (y) directions, respectively.

Current implementations of MTM rely on “infinite” rods and split-ring resonators (SRRs), as shown in **Figure 14**, to achieve a negative permittivity and a negative permeability, respectively.

The MTM, built from the rings (loop antenna) and rods (small electric dipole) from microscopic view, is seen as a homogeneous effective medium, characterized by the material parameters ε and μ . This approach is possible because the sizes of the rings and rods as well as the distances between them are very small compared to the wavelength.

The shapes of the rings, their effective radii, width of metallization and many other factors directly translate into MTM properties: the position of the resonance frequency and plasma frequency that control directly into frequency bandwidth in which appear the negative values of $-\varepsilon$ and/or $-\mu$ [44]. Therefore, the design and optimization of the geometry of the rings have still been a current area of research.

For lossy DNG MTM material, negative permeability and permittivity can be determined by using the Drude model [44] as follows:

$$\varepsilon(\omega) = \varepsilon_0 \left[1 - \frac{\omega_{pe}^2}{\omega(\omega - j\Gamma_e)} \right] \quad (14)$$

$$\mu(\omega) = \mu_0 \left[1 - \frac{\omega_{pm}^2}{\omega(\omega - j\Gamma_m)} \right] \quad (15)$$

where ω_{pe} , ω_{pm} and Γ_e , Γ_m mean plasma frequency and the damping frequency, respectively.

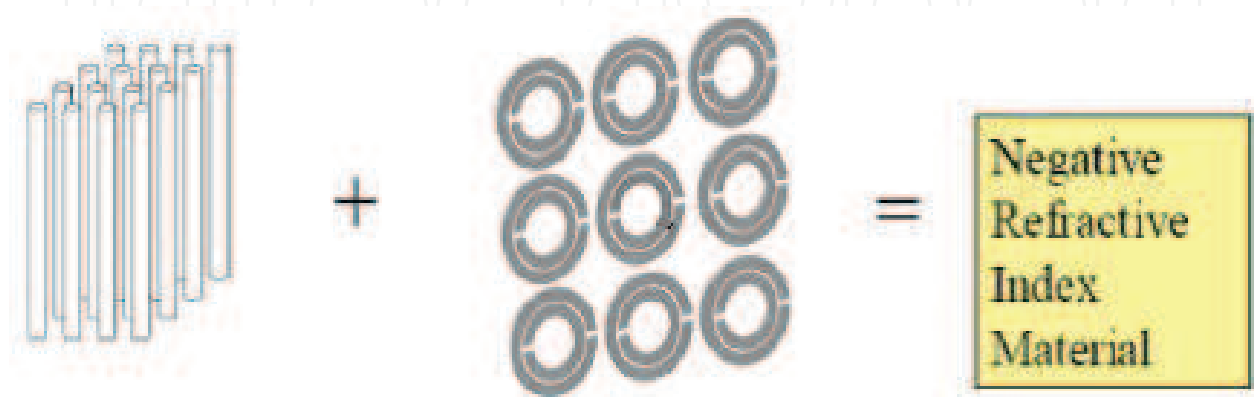


Figure 14. Synthesis of DNG MTM.

Analysis based on the Drude model can be implemented in the FDTD method by introduction of appropriate density of electric current to the equations that describe their temporal behaviour. For modelling of E (M) NG MTM, the dispersion permittivity or permeability is replaced by the frequency-independent constants.

Many research groups in the world have been studying various aspects of this class of MTM, where a number of ideas and suggestions for future applications of these materials have been proposed. Initially, it was to enter the isotropic material parameters, namely scalar permeability (ϵ) and scalar permeability (μ). The isotropic approximation, however, is valid for single polarization of excitation of MTM containing rings in the two dimensions, such as in the original experiment. Later versions of the MTM were built by using rings in only one direction only, which violates the principle of isotropy and creates a MTM internally anisotropic. The relative parameters of the material, therefore, must be described in the form of tensors, characterizing the model of biaxial media.

3.4. Negative refractive index

The phenomenon of EM-waves refraction with a negative refraction coefficient has been studied taking into account the EM wave scattering incident at any angle to the boundary surface of the DPS-DNG materials, as shown in **Figure 15**.

Enforcing the electromagnetic boundary conditions at the interface, one obtains the law of reflection and Snell's Law from phase matching:

$$\theta_{ref1} = \theta_{ref2} \quad (16)$$

$$\theta_{trans} = \text{sgn}(n_2) \sin^{-1} \left(\frac{n_1}{|n_2|} \sin \theta_{inc} \right) \quad (17)$$

It should be noted that if the refractive index of medium is negative, it means the angle of refraction, in accordance with of the Snell's law, should be "negative". This suggests that the refraction is abnormal, and the angle of refraction is on the same side of the normal to the interface as the incident wave angle is (see **Figure 16**).

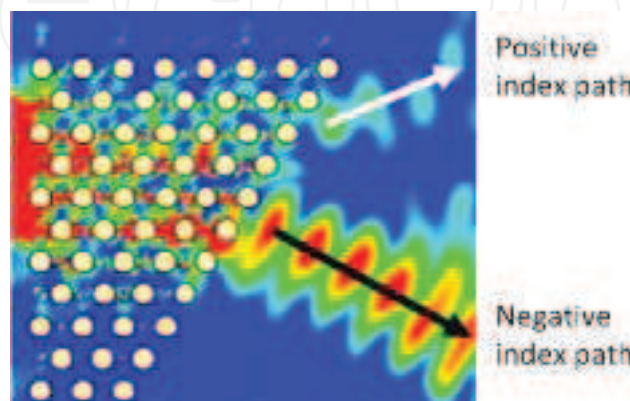


Figure 15. Refraction properties of the resonant MTM.

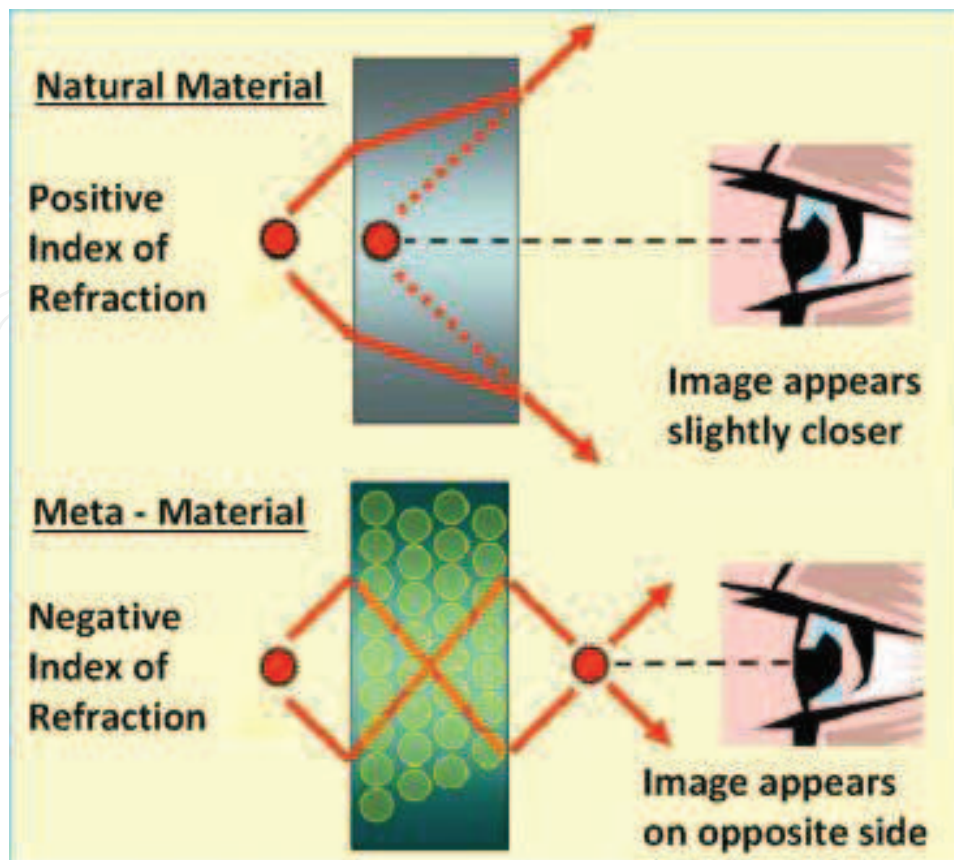


Figure 16. Imaging with DPS and DNG materials.

3.5. Metamaterials of high impedances surface

MTMs with high-impedance surface HIS are also known as artificial magnetic conductors that drew the attention of investigators in the past few years [5]. These surfaces have a reflectivity coefficient $\Gamma \cong +1$ when plane wave illuminate it, in contrast to the typical $\Gamma \cong -1$ in the case of the surfaces of perfectly electrically conductive (PEC). These structures can meet the interesting application in the design of the antenna [46] and the thin absorbing screens.

For example, a dipole antenna located above such HIS MTM has an image current with the same phase as the current on the host dipole, such phenomena increase the level of EM-waves radiation as well as the efficiency of dipole antenna. Several different types of HIS as the modified ground planes have been studied by a number of research groups [46, 47].

Because the magnetic conductive surfaces do not occur naturally, it is necessary to create them artificially to meet the surface conduction properties in selected frequency ranges. This can be achieved by utilizing the resonant properties of inclusions on the non-conducting substrate host layer in parallel with the ground plane. Near resonance frequency on inclusions of strong surface currents is induced and together with the conductive ground plane, this structure behave as an equivalent magnetic conductor PMC also known as HIS, for a frequency range corresponding to the vicinity of a resonance of the surface.

Periodical MTM can be divided into two groups: (1) the three-dimensional volumetric structure and (2) the two-dimensional surfaces. The latter, have such advantages as low profile, low weight and low-cost production. Therefore, such a solution is proposed in mobile wireless communication systems [4].

The artificial surfaces have been testing for many years and so far have developed such as frequency-selective surfaces (FSSs) [9]; artificial soft and hard surfaces LIS and HIS, respectively [10], and micro-machined substrates [4]. Recently, the planar EBG surfaces are proposed [4], which have some specific properties relative to incident waves, respectively when

- i. an incident wave is a surface wave ($k_x^2 + k_y^2 \geq k_0^2$, where the k_x and k_y are wavenumbers in horizontal direction, while the k_0 is the wavenumber in a free space), analyses of such structure shows if it has the property of bandgap (EBG) material, it means that a surface wave cannot propagate along it for any incident angle and polarization, and
- ii. an incident wave is plane wave ($k_x^2 + k_y^2 < k_0^2$), the reflection coefficient of a material is equal $\Gamma = +1$ for a specific frequency, which resembles to the PMC that does not exist in nature. The simplest example of a textured electromagnetic surface is a metal plate, in which milling out the grooves (corrugations) with a depth of $d = \lambda/4$ [32, 38], is shown in **Figure 17a**.

This structure depending on the polarization and direction of propagation of the EM-wave is described as a soft or hard surface [4]. The action of such surface, relative to EM-fields we can understand treating the corrugations as transmission quarter-wavelength lines, short-circuited at the bottom of each groove, which is transformed in the open-circuit at the top of the surface. This provides a high impedance (hard surface) for electric fields polarized perpendicular to the grooves and low impedance (soft surface) for parallel-polarized electric fields. Soft LIS and hard HIS surfaces are used in various applications, such as modification of radiation patterns of aperture antennas (open-end waveguide, horn, parabolic dish, slot, microstrip, etc.), the elimination of surface currents between the radiating elements of flat antenna arrays

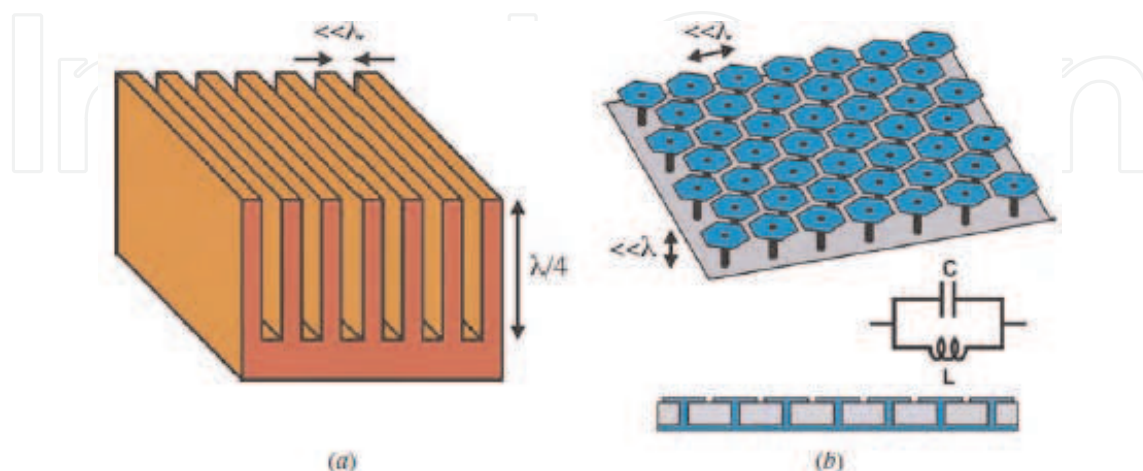


Figure 17. A traditional corrugated surface consists of a metal slab with narrow quarter-wavelength long slots (a) and a high-impedance surface is built as a thin two-dimensional lattice of plates attached to a ground plane by metal-plated vias (b).

(minimization of mutual couplings) or modelling of parameters of the edges on which the diffraction of EM-waves occur.

More compact metal constructions, with a thickness much less than $\lambda/4$, that change the boundary conditions for the EM-wave, were proposed in Ref. [4]. They are built of metal in the shape of mushrooms (flat metal square over short-pin), about the size of a much smaller wavelength, as shown in **Figure 17b**. Each of these “mushrooms” can be modelled as an LC-resonant circuit. The structure has reduced thickness that is achieved by means of capacitive load. These materials provide high-impedance boundary conditions for both polarization and all directions of propagation of waves, and act as hard surfaces. EM waves reflecting from such surface do not change the phase, $\varphi = 0$, as opposed to reflection from the perfect conductor, for which $\varphi = \pi$.

It is sometimes known as artificial magnetic conductor, because tangential component of magnetic field H is equal to zero on the surface, such as the E-field tangential component on the surface of a perfect conductor (metal). In addition to the unusual behaviour of phase of the reflected EM-wave, these materials have a bandgap of the surface wave in which they prevent the occurrence of TM and/or TE-surface waves. Hence, it can be treated as a kind of bandgap structure for electromagnetic waves (EBG) or photonic crystal for surface waves [4]. Although the surface waves cannot propagate in such structures, leaky TE-modes of EM-wave can propagate within the bandgap, which can be useful in some applications.

One of the possibilities to form inclusions that are resonant but have an electrically small footprint at their resonant frequency is the use of the space-filling curves of fractal geometry.

4. Metamaterials based on fractal geometries

At the beginning of the twenty-first century appeared the new MTM configurations, based on fractal geometry. This allows for a significant reduction in the size of individual cells, which are built of artificial materials, which, in turn, translates into higher homogeneity of the material and the reductions in the profile of artificial ground [1].

Many shapes have been proposed for artificial magnetic materials [6]. **Figure 18** shows some of these topologies.

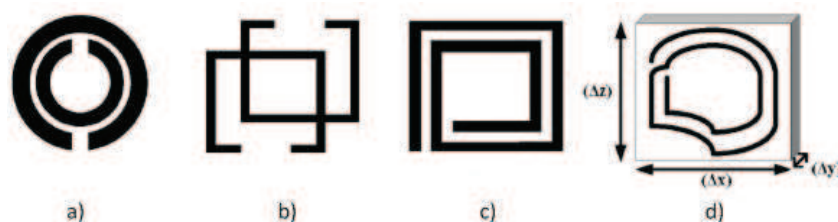


Figure 18. Some particles used in magnetic MTM: SRR (a), meta solenoid (b), split spiral (c), and ring with arbitrary shape (d).

New structures, despite of the other shapes, provide unchanged mechanism of its operation. When the resonant-cells are immersed in the media, where there an external magnetic field H_{ext} exists, the changes in magnetic flux density, covered by these inclusions in the shape of the rings, induces in them the electromotive force (*emf*). Voltages of *emf* cause the current flow on the ring surface, which, in turn, induces a dipole magnetic moment. In turn, the dipole magnetic moment is the source of the effective permeability. We will try to determine the magnetic moments of any shape cell-inclusions (see **Figure 18d**). The electromagnetic properties of the proposed structures were examined in detail and compared to a property of spiral-shaped cells.

4.1. MTM based on Hilbert fractal curves

In this chapter, we introduce combination of the square spiral loop configuration with fractal Hilbert curves as inclusions for artificial magnetic material to further increase the miniaturization potential (**Figure 19**).

It is shown that by using third-order fractal Hilbert curves, inclusions as small as $\lambda/55$ (**Figure 19c**) (λ the wavelength in the host dielectric at the resonance frequency) can be realized.

To analytically predict the behaviour of Hilbert curve inclusions, the equivalent circuit model parameters are provided in Ref. [6]. The unit cell shown in **Figure 19c** has dimension (as in **Figure 18d**) has dimension Δx , Δy and Δz , in the x, y and z directions, respectively. The resultant permeability is described by following expression [6]:

$$\mu_{rf} = 1 - \frac{S}{\Delta z \Delta x} \frac{j\omega L_{eff}}{R_{eff} - \frac{1}{\omega C_{eff}} + j\omega L_{eff}} \quad (18)$$

where ω is the external field frequency, S is the surface enclosed by inclusion, and R_{eff} , L_{eff} and C_{eff} are equivalent circuit model components, derived in [6] for the proposed Hilbert curve inclusions.

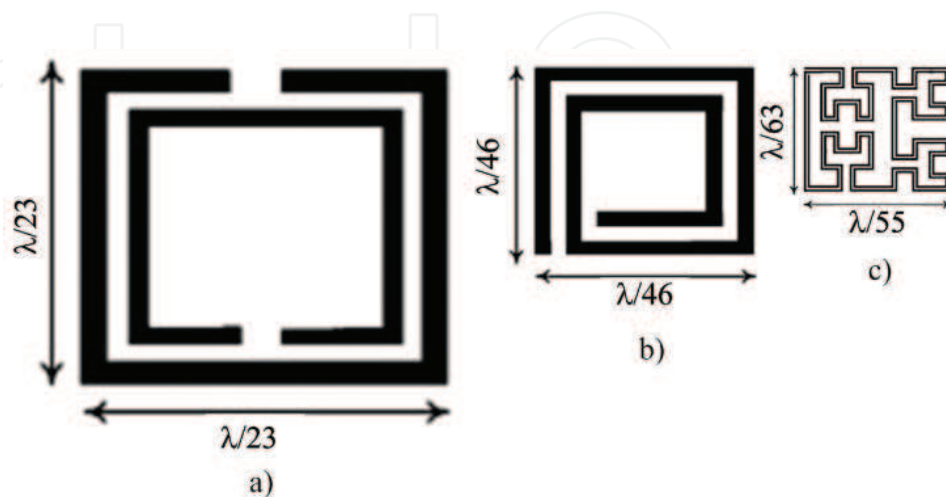


Figure 19. A unit cell of inclusion with SRR (a), square spiral (b) and third order Hilbert fractal (c), respectively.

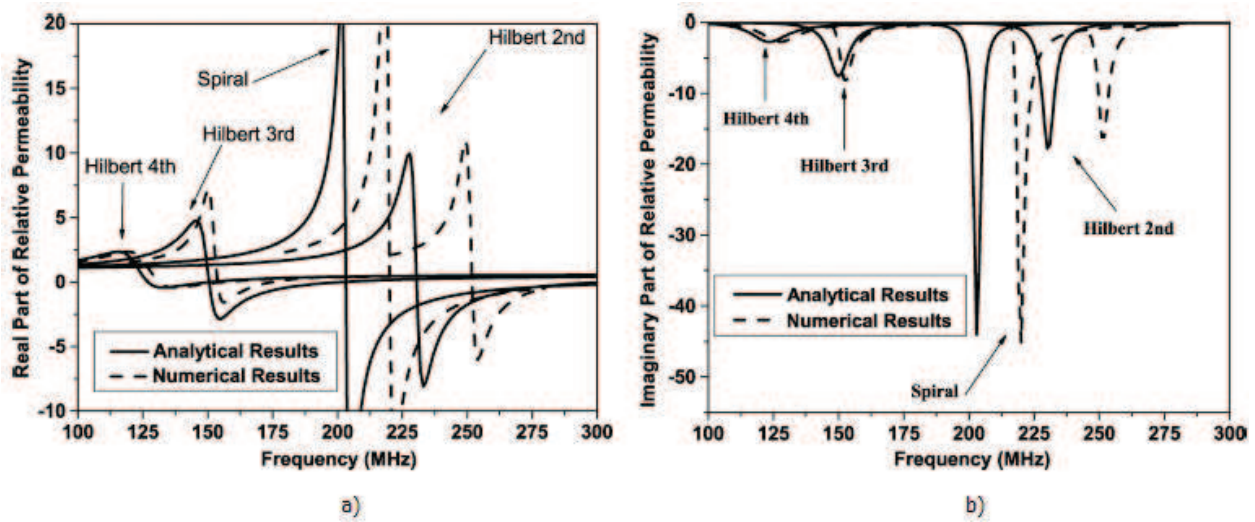


Figure 20. Real (a) and imaginary (b) part of permeability of MTM with Hilbert fractal curve inclusion.

The relative permeability of different order Hilbert fractal curve unit cells was derived in Ref. [6] and shown in **Figure 20**.

Figure 20 shows of the permeability plots versus frequency of single cell of MTM structure in the form of the Hilbert fractal curve (**Figure 19c**). They are quite similar to the characteristics of the MTM cell in the form of a square spiral (**Figure 19b**), which was used before fractals [6]. It should be noted that the external dimensions of fractal cells ($\lambda/55$) are much smaller than the dimensions of the split spiral cell ($\lambda/46$), having the same copper strip width w and separation s between them ($s = w = 0.127$ mm), as well as the host dielectric substrate ($\epsilon_r = 3.38$, $\tan\delta = 0.0027$). For higher iterations of the Hilbert fractal, the differences become greater.

In addition, as shown in **Figure 20**, when the number of iterations of the Hilbert fractal is increased, the permeability plot becomes smoother. Therefore, the use of fractal structures causes decrease in changes of the permeability depending on the frequency, which, in turn, reduces the coefficient of dispersion in an artificial medium. For frequencies below the resonance, the imaginary part of the permeability takes larger values for fractal Hilbert inclusions than for rectangular spiral cells. Moreover, the Hilbert cells with higher iterations have higher values for the imaginary component μ of the permeability.

Therefore, at frequencies below resonance, the Hilbert inclusions bring greater losses compared to the spiral cells. It has been shown that using four-order fractal Hilbert, we can build a very small MTM cells, with dimensions of the order of 0.014λ in the dielectric substrate. This size corresponds to 63% of the size of the spiral cell and 32% of the size of the SRR cell (see **Figure 19**).

4.2. MTM composed of fractal tree sphere

Properties of an artificial dielectric MTM depend primarily on the type of inclusions, as well as their distribution in the host environment. Some types of cell geometry considered in the past to build for artificial dielectric materials include small dipoles and loops. In this chapter,

we will consider the possibility of using for this purpose the fractal tree, which could approximate the sphere [7]. It will be a sort of a combination of aspects of both the geometry of the dipole and the sphere.

MTMs will be considered here that are composed of a new type of molecule called fractal tree sphere. A fractal sphere is collection of symmetric self-similar fractal tree dipoles arranged to form a sphere-like structure as illustrated in **Figure 21**.

The effective dielectric constant of artificial dielectric MTM is evaluated from effective electric and magnetic polarizabilities, respectively:

$$\mathbf{p} = \varepsilon (\bar{\bar{a}}_{ee} \mathbf{E} + \bar{\bar{a}}_{em} \eta \mathbf{H}) \quad (19)$$

$$\mathbf{m} = \frac{\bar{\bar{a}}_{me}}{\eta} \mathbf{E} + \bar{\bar{a}}_{mm} \mathbf{H} \quad (20)$$

The effective dielectric constant of fractal sphere MTM is evaluated as follows:

$$\varepsilon_{eff} = \varepsilon \frac{(1 + 0.66 N a_{ee}) (1 - 0.33 N a_{mm}) - 0.22 N^2 a_{em}^2}{(1 - 0.33 N a_{ee}) (1 - 0.33 N a_{mm}) + 0.11 N^2 a_{em}^2} \quad (21)$$

where N is the inclusion volume density.

The real and imaginary parts of the effective constant for the three iterations of the fractal sphere are shown in **Figure 22**.

The plots of an effective dielectric constant for an artificial dielectric MTM consisting of conventional dipole inclusions are inserted in **Figure 22a, b** for comparison purposes. In this case, maximum number N_{max} of inclusions that can be placed in a cubic meter volume without intersection was considered. It could be seen that each, successive iteration of the fractal tree sphere molecules produces a characteristic downward shift in the corresponding peak value of the ε_{eff} . Also, it is seen that a medium composed of third iteration fractal tree spheres behaves as a dual-band artificial dielectric MTM. It has been shown that fractal

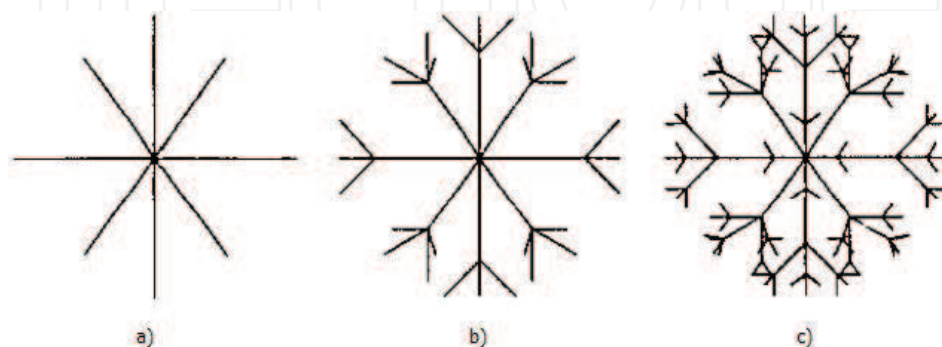


Figure 21. Fractal trees of first (a), second (b), and third iteration (c), approximating the spheres, as viewed along any axes.

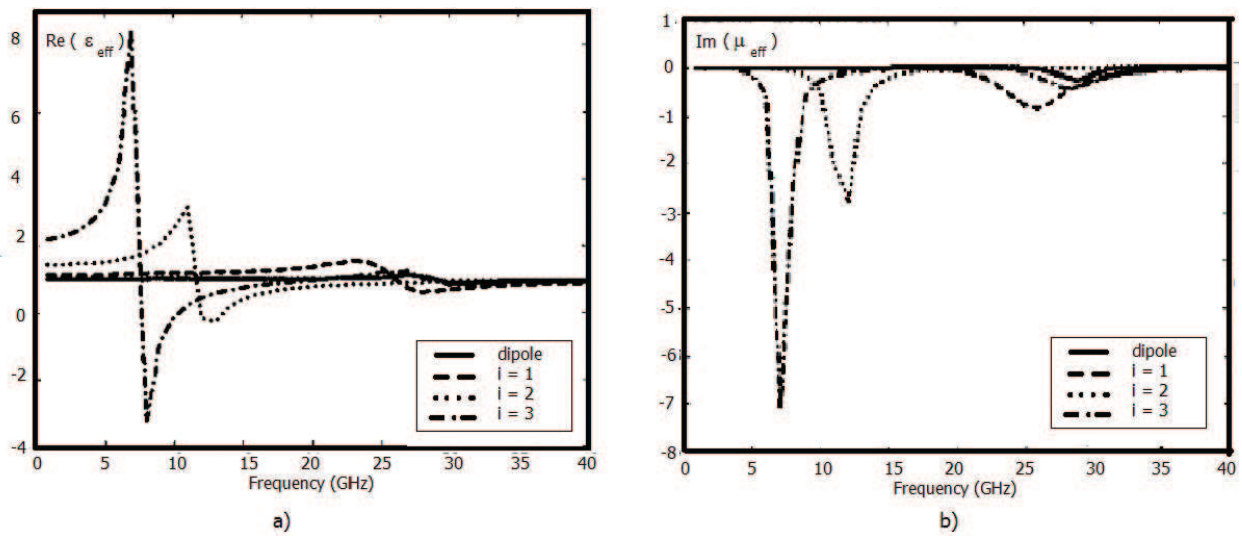


Figure 22. Real (a) and imaginary (b) part of effective dielectric constant of the fractal tree sphere.

spheres have a lower resonant frequency than those solid spheres of the same physical size. These properties have been exploited to develop a new class of low-frequency multiband MTM.

4.3. Fractal self-space-filling curve high-impedance ground planes

Because the magnetic conductive surfaces do not occur naturally, as mentioned earlier, it is necessary to artificially create such a surface that meet the requirements in the specified frequency range [4]. This can be achieved using the resonant properties of inclusions in non-conducting layer of the substrate in parallel with a conductive plane host substrate. Near resonance of the inclusions, the strong currents are induced on the surface of the material, which causes the material to behave as an equivalent magnetic conductor. One of the possible inclusions, which possess the resonant properties and are electrically small ($\ll \lambda$) is the use of self-filling fractal curves.

The self-filling of the surfaces curves are, in general, the continuous maps of the area by an interval $[0, 1]$ on standardised square $[0, 1] \times [0, 1]$. In the year 1890, Peano first proposed the self-filling curve, now called the Peano curve [12]. In 1891, David Hilbert introduced its version of the same—filling curve [4]. The curves are iterative, both fill the entire surface, when the number of iterations (so called curve order) tends to infinity; this means that the curves pass through each points on the surface of the square. While both curves pass through each point on the surface for $i = \infty$, it realizes this in a quite different way, as you can see for the first three iterations of the Peano curves and Hilbert, shown in Figure 23.

These curves offer certain attractive properties; that is, a structure of this shape can be made from an electrically long metallic wire compacted within a very small footprint area. As the iteration order of the curve increases, a space-filling curve may maintain its footprint size

while its length increases. Moreover, these space-filling geometries can be planar structures, thus allowing for ease of fabrication.

The total lengths of these Peano, D_P and Hilbert, D_H , curves as a function of the iteration order i , are given by Eqs. (22a) and (22b), respectively.

$$D_P = L \frac{3^{2i} - 1}{3^i - 1} \quad (22a)$$

$$D_H = L \frac{2^{2i} - 1}{2^i - 1} \quad (22b)$$

where L is a linear side length of the curve.

As you can see, the Peano curve has a higher compression ratio (e.g. greater total length) than Hilbert curve for a fixed order. The space-filling curve elements can resonate at frequencies where the curve side dimension can be considered as electrically very small. The higher order curve has a lower resonant frequency; thus, it takes up less surface area in relation to the resonant wavelength. The cost of the implementation of the compact resonant is seen in narrower bandwidth.

This effect has also been observed in the design of electrically small antenna based on Peano or Hilbert curves [4]. The element in the form of Peano curve with the same surface and order of iteration as an element of a Hilbert curve has a much lower resonance frequency, at the expense of a much narrower bandwidth, due to the higher compression ratio of Peano curve.

To construct a high impedance surface, HIS, the Peano curve elements can be placed in a planar, 2D array as shown in **Figure 24**.

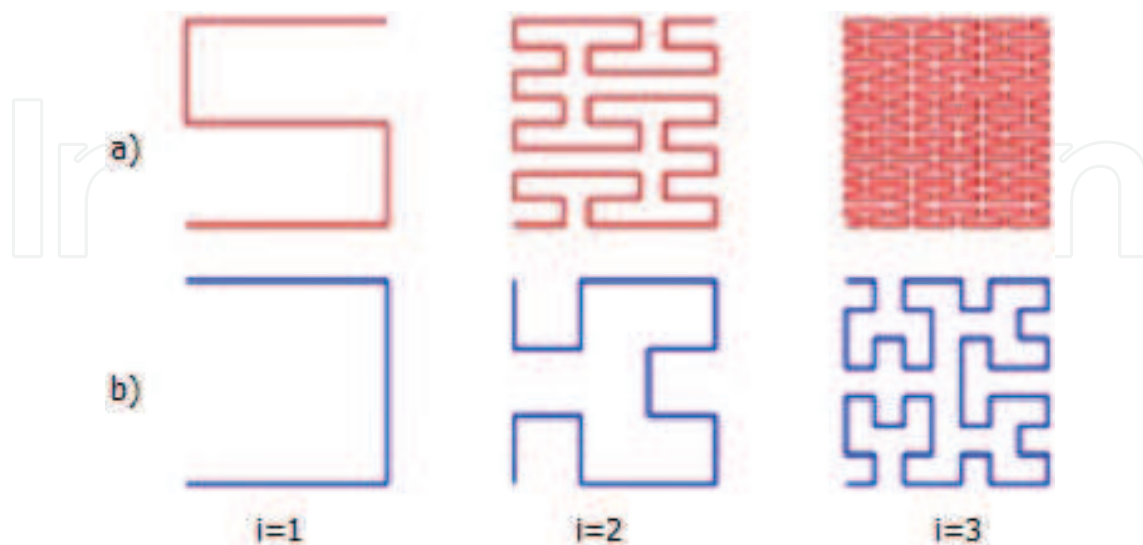


Figure 23. Peano (a) and Hilbert (b) fractal space-filling curves for first three iterations.

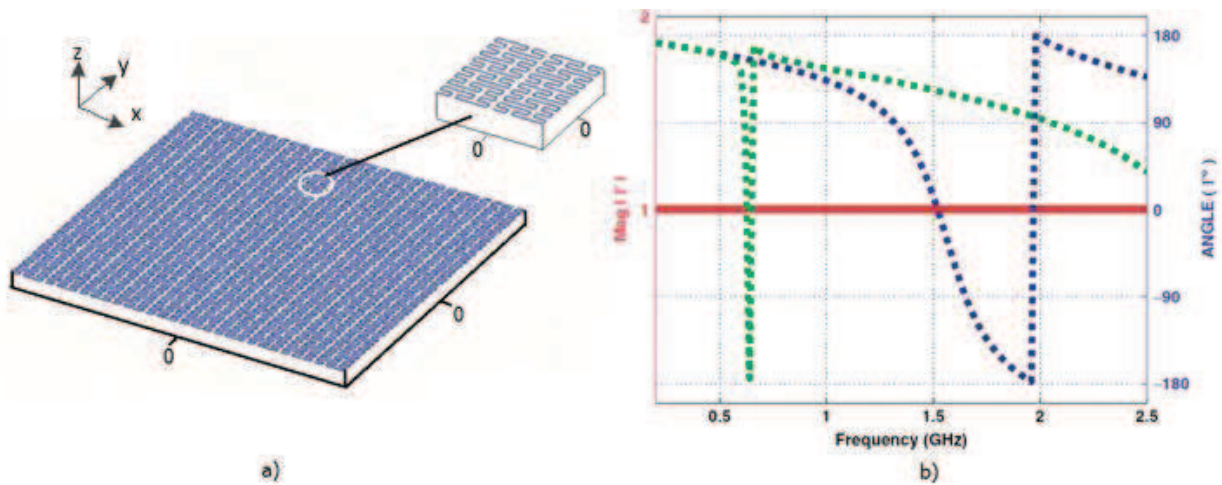


Figure 24. The HIS build-up of second order Peano fractal above conducting ground plane (a) and reflection coefficient for normally incident wave with polarizations in x- and y-planes (b).

In this case, each element was designed as a thin metallic strip with a strip width of 0.5 mm. The footprint dimensions remain identical (30×30 mm). The Peano array was placed a distance (15 mm) above a conducting ground plane of infinite extent. The supporting dielectric substrate is considered air here, although any other dielectric can be considered.

A separation distance was of 3.75 mm between each Peano curve inclusion within the array. This distance was chosen to be equal to the length of a single section of the curve itself. **Figure 24b** shows the magnitude and phase of the reflection coefficient Γ versus frequency. For the frequency of $f_{HIS} = 1.53$ GHz, in the case of the incident EM-wave polarized in the x-direction, where phase is $\varphi = 0$ over the entire surface of HIS, above the ground plane the reflection coefficient is $\Gamma = +1$; that is, it satisfies the conditions of a magnetic conductor MTM. Beyond the resonance across the entire surface of HIS, the reflection coefficient is $\Gamma = -1$ and, therefore, behaves as an electric conductor. Note that the cells of MTM in the form of a fractal Hilbert curve are of external sizes appropriately as $0.063 \lambda_{HIS}$ and $0.153 \lambda_{HIS}$ and thickness of substrates around $0.031 \lambda_{HIS}$ and $0.076 \lambda_{HIS}$, respectively, at f_{HIS} (**Figure 24b**). That is, these cells are small electrically for both polarities [4].

MTM cells in the form of self-filling Peano and Hilbert curves can offer a lot of interesting features in electromagnetic applications. One of the most interesting features is the ability to work in resonant conditions where electrical dimensions of area filled by the curve are very small. This means that the self-filling curves can be excellent candidates for building surface and bulk media, where electrically small inclusions are desirable, for the design of specific electromagnetic properties of MTM. One of the most important uses of HIS surface is to use them to improve the performance of low-profile antennas.

4.4. EBG structures based on fractal cells

Recently, a novel electromagnetic bandgap (EBG) structure design based on fractal, the Sierpinski gaskets are proposed. They are arranged by repetition of 60° each to introduce the hexagonal unit

cells [8]. By changing the gaps G_2 between two adjacent Sierpinski triangles inside EBG unit cell, it can separately introduce two EBG structures that have broadband and dual band-gap. Single cell geometry exhibits symmetry in six-planes, which makes it polarisation angle-independent. The proposed EBG structures, photo-etched on the FR4 microwave laminate ($\epsilon_r = 4.4$, $h = 1.6$ mm, $\tan\delta = 0.02$) are shown in **Figure 25**.

The Sierpinski gasket is a well-known fractal. Dark parts in this figure represent the metallic periodic structure, which is etched on a dielectric substrate. Unit cell dimensions are $W = 10$ mm, $W_1 = W - 2(G_1 + G_2)/\sqrt{3}$, $W_2 = 0.5 W_1$, $W_3 = 0.25 W_1$, $W_4 = W_1/8$, $G_1 = 1$ mm, $G_2 = 0.5$ mm, and the metallization thickness is $18 \mu\text{m}$. The Sierpinski gasket triangles are arrangement to

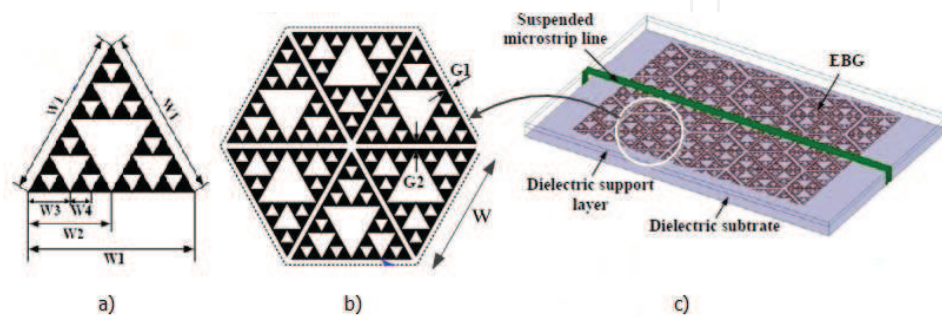


Figure 25. Sierpinski gasket fractal triangle (a), two-dimensional sketch of unit hexagonal cell (b) and three-dimensional of EBG array (c).

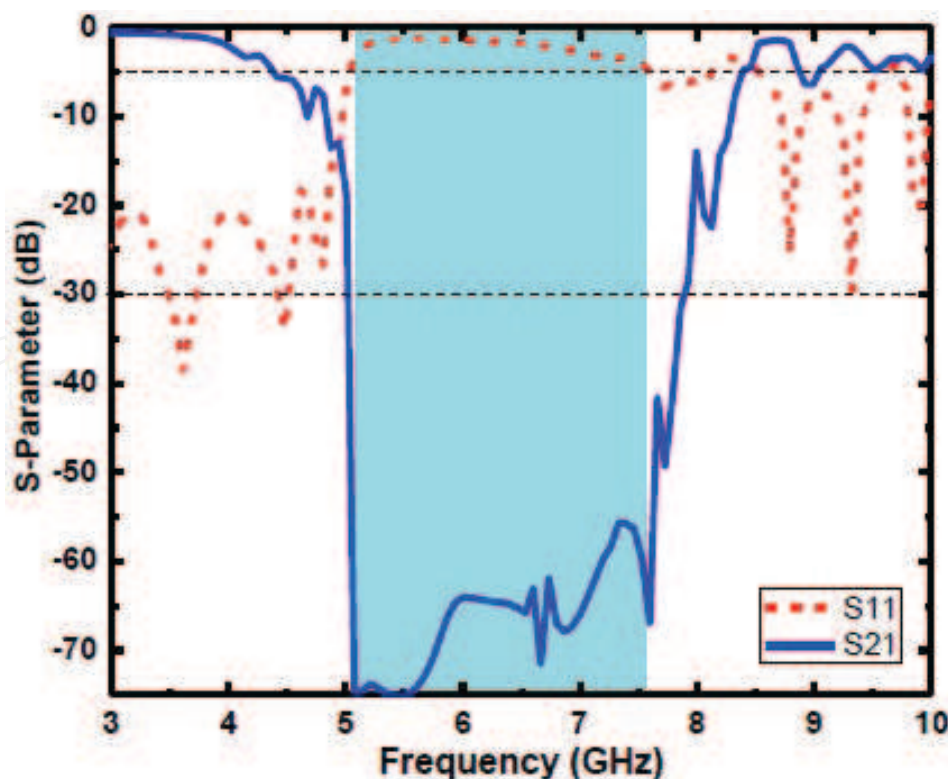


Figure 26. Operation bandwidth of HIS MTM based on an array of hexagonal cells of Sierpinski fractal triangles.

repeat each 60° . The resonance frequencies and the EBG operation bandwidth can be modified by changing the width and the gap G_1 between the hexagonal lattices. Moreover, by changing the gap G_2 between Sierpinski triangles units, it can introduce two EBG structures separately. The first one, which is called broadband EBG structure (BEBG), has a broader bandgap with the value of G_2 up to 0 mm. The simulation results of the EBG structures based on Sierpinski are shown in **Figure 26**.

The EBG structure has a bandgap, in the frequency range from 5.07 to 7.58 GHz, for $G_2 = 0.5$ mm. A wider bandwidth of operation frequency, with smaller EBG cell-size was obtained due to significantly reduced capacity C of an equivalent parallel resonant circuit, as well as limitation of the relative permittivity.

Author details

Wojciech Jan Krzysztofik

Address all correspondence to: wojciech.krzysztofik@pwr.edu.pl

Faculty of Electronics, Wroclaw University of Science & Technology, Wroclaw, Poland

References

- [1] Youefi L, Ramahi OM. Artificial magnetic materials using fractal hilbert curves. *IEEE Transactions on Antennas and Propagation*. 2010;**58**(8):2614-2622. DOI: 10.1109/TAP.2010.2050438
- [2] de Araujo HX, Barbin SE, Kretly LC. The use of metamaterial technology to improve a GTEM chamber. In: *International Microwave Optoelectronics Conference (IMOC), 2013 SBMO/IEEE MTT-S*. 2013. pp. 1-5. DOI: 10.1109/IMOC.2013.6646506
- [3] Krzysztofik WJ. Antenna properties improvement by means of modern technology - metamaterials as a modified substrate and/or superstrate. In: *MIKON'2014 20th International Conference on Microwaves, Radar and Wireless Communications*. 2014. pp. 1-4. DOI: 10.1109/MIKON.2014.6899975
- [4] Engheta N, Ziolkowski RW. *Electromagnetic Metamaterials: Physics and Engineering Explorations*. USA: Wiley-IEEE Press; 2006
- [5] McVay J, Engheta N, Hoorfar A. High impedance metamaterial surfaces using Hilbert-curve inclusions. *IEEE Microwave and Wireless Components Letters*. 2004;**14**(3):130-132. DOI: 10.1109/LMWC.2003.822571
- [6] Yousefi L, Ramahi OM. New artificial magnetic materials based on fractal Hilbert curves. *International Workshop on Antenna Technology: Small and Smart Antennas Metamaterials and Applications*, 2007. IWAT '07. 2007. pp.237-240. DOI: 10.1109/IWAT.2007.370119

- [7] Facchinetti MJ, Werner DH. Metamaterials composed of fractal sphere molecules. In: IEEE Press, editor. IEEE Antennas and Propagation Society International Symposium, IEEE APS-2003; 2003. pp. 102-105. DOI: 10.1109/APS.2003.1217411
- [8] Phuong HNB, Chien DN, Tuan TM. Novel design of electromagnetic bandgap using fractal geometry. *International Journal of Antennas and Propagation*. 2013;**2013**:1-8/162396. DOI: 10.1155/2013/162396
- [9] Krzysztofik WJ. Fractal geometry in electromagnetics applications - from antenna to metamaterials. *Microwave Review*. 2013;**19**(2):3-14. ISSN: 14505835.
- [10] Mandelbrot BB. *The Fractal Geometry of Nature*. New York: W.H. Freeman; 1983.
- [11] Zaad MZ, Ali M. A miniature hilbert PIFA for dual-band mobile wireless applications. *IEEE Antennas and Wireless Propagation Letters*. 2005;**4**:59-62
- [12] Best SR, Morrow JD. The effectiveness of space-filling fractal geometry in lowering resonant frequency. *IEEE Antennas and Wireless Propagation Letters*. 2002;**1**:112-115
- [13] Kritikos HN, Jaggard DL, editors. *Recent Advantages in Electromagnetic Theory*. New York: Springer-Verlag; 1990
- [14] Sachendra SN, Jain M. A self-affine multiband antenna. *IEEE Antennas and Wireless Propagation Letters*. 2007;**6**:110-112
- [15] Krzysztofik WJ. Printed multiband fractal antennas. In: Sanchez-Hernandez DA, editors. *Multiband Integrated Antennas for 4G Terminals*. 1st ed. Norwood, MA, USA: Artech House, Inc; 2008. pp. 95-150.
- [16] Krzysztofik WJ. Modified sierpinski fractal monopole for ISM handset applications. *IEEE Transaction on Antenna and Propagation*. 2009;**57**(3)
- [17] Krzysztofik WJ. Fractal monopole antenna for dual-ISM-bands. In: *European Microwave Conference (EuMC-2006)*; UK, Manchester; 2006. pp. 1461-1464
- [18] Krzysztofik WJ. *Terminal antennas of mobile communication systems – some methods of computational analysis*. Wroclaw, Poland: Wroclaw University of Science and Technology Press; 2011. p. 239
- [19] Krzysztofik WJ, Baranski M. Fractal structures in antenna technology. *Scientific Books of Gdansk University of Technology, Series: Radio Communication, Radiobroadcasting & Television*. 2007; Gdansk, Poland (**1**); 2007. pp. 381-384
- [20] Krzysztofik WJ. Fractal antenna for WLAN/bluetooth multiple-bands applications. In: *EUCAP 2009, 3rd European Conference on Antennas and Propagation*; 2009; Berlin, Germany; 2009. pp. 2407-2410
- [21] Krzysztofik WJ, Komaryczko M. Fractal antennas in terminals of mobile communication systems. In: *KKRRiT-2004 National Conference on Radio Communication, Radiobroadcasting & Television*; 2004; Warsaw, Poland; 2004. pp. 436-439

- [22] Falconer KJ. Mathematical Foundations and Applications. 2nd ed. Chinchester, New York: John Wiley & Sons; 2003.
- [23] Werner DH. Fractal radiators. In: Proceedings of the 4th Annual 1994 IEEE Mohawk Valley Section Dual-Use Technologies & Applications Conference; 23–26 May 1994; New York: SUNY Institute of Technology at Utica/Rome; 1994. pp. 478-482
- [24] Puente C, Baliarda CP, Romeu J, Cardama A. The koch monopole: A small fractal antenna. IEEE Transactions Antennas and Propagation. 2000;**AP-48**(11):1773-1781
- [25] Werner DH, Bretones AR, Long BR. Radiation characteristics of thin-wire ternary fractal trees. Electronics Letters. 1999;**35**(8):09-10
- [26] Rahmat-Samii Y, Gianvittorio JP. Fractal antennas: A novel antenna miniaturization technique and applications. IEEE Antenna's and Propagation Magazine. 2002;**44**(1):20-36
- [27] Werner DH, Gangul S. An overview of fractal antenna engineering research. IEEE Antennas and Propagation Magazine. 2003;**45**(1):38-57
- [28] Puente C, Romeu J, Pous R, Garcia X, Benitez F. Fractal multiband antenna based on the sierpinski gasket. IEE Electronics Letters. 1996;**32**(1):1-2
- [29] Rahim MKA, Jaafar AS, Aziz MZAA. Sierpinski gasket monopole antenna design. In: Asia-Pacific Conference on Applied Electromagnetic; 20–21 December 2005; Malaysia; 2005. pp. 49-52
- [30] Guterman J, Mortira AA, Peixeiro C. Microstrip fractal antennas for multistandard terminals. IEEE Antennas and Wireless Propagation Letters. 2004;**3**:351-354
- [31] Mittra R. A critical Look at the Performance Enhancement of Small Antennas using Metamaterials. International Workshop on Antenna Technology: Small and Smart Antennas Metamaterials and Applications, 2007, IWAT'07, pp.7-10, DOI: 10.1109/IWAT.2007.370069
- [32] Veselago V G. The electrodynamics of substances with simultaneously negative values of ϵ and μ . Soviet Physics Uspekhi. January–February 1968;**10**:509-514
- [33] Cui T.J. , ed., Metamaterials. Springer Science+Business Media B.V. Netherlands, DOI: 0.1007/978-1-4419-0573-4_13, 2010
- [34] Falcone F., et al. Babinet principle applied to the design of metasurfaces and metamaterials. Physical Reviews Letters. 2004;**93**:197401
- [35] Abdalla MA, Hu, Z. Comapct and tunable metamaterial antenna for multi-band wireless communication applications. In: IEEE International Symposium on Antennas and Propagation (APSURSI); July 2011; pp. 1054-1057
- [36] Zhang H, Ziolkowski RW, Xin H. A compact metamaterial-inspired mmW CPW-Fed antenna. In: IEEE International Workshop on Antenna Technology (iWAT); 2009; pp. 1-4

- [37] Mei ZL, et al. A half Maxwell fish-eye lens antenna based on gradient-index metamaterial. *IEEE Transactions on Antennas and Propagation*. January 2012;**60**(1):398-401
- [38] Bose JC. On the rotation of plane of polarization of electric waves by a twisted structure. *Proceedings of Royal Society*. 1898;**3**:146-152
- [39] Lindell IV, Sihvola AH, Kurkijarvi J. Karl F. Lindman: The last Hertzian, and a Harbinger of electromagnetic chirality. *IEEE Antennas and Propagation. Magazine*. 1992;**34**(3):24-30
- [40] Cui TJ, Smith DV, Liu R. *Metamaterials: Theory, Design and Applications*. New York, US: Springer; 2010.
- [41] Araujo HX, Kretly LC. The effect of metamaterial patterning to improve the septum GTEM chamber performance. In: 29th Progress in Electromagnetics Research Symposium; March 2011; Marrakesh. 2011
- [42] Cui T.J. Electromagnetic metamaterials: Recent advances on the theory, experiments, and applications. 2009 International Conference on Microwave Technology and Computational Electromagnetics (ICMTCE 2009), DOI: 10.1049/cp.2009.1248, pp. 12-13, 2009
- [43] Hrabar S, et al. Application of wire-based metamaterials for antenna miniaturization. In: 3rd European Conference on Antennas and Propagation (EuCAP) 2009; pp. 620-623
- [44] Shelby RA, Smith DR, Schultz S. Experimental verification of a negative index of refraction. *Science*. April 2001;**292**(5514):77-79
- [45] Pendry JB. Negative refraction makes a perfect lens. *Physical Review Letters*. October 2000;**85**(18):3966-3969
- [46] Sievenpiper D, Zhang L, Broas RFJ, Alexopolous NG, Yablonovitch E. High-impedance electromagnetic surfaces with a forbidden frequency band. *IEEE Transactions on Microwave Theory and Techniques*. 1999;**47**:2059-2074
- [47] Zhang Y, Hagen J, Wiesbeck W. Patch array as artificial magnetic conductors for antenna gain improvement. *Microwave and Optical Technology Letters*. 2002;**35**(3):172-175
- [48] Isbell D. E., "Log Periodic Dipole Arrays", *IRE Trans.*, Vol. AP-8, No. 3, May 1960, pp. 260-267.

